Technische Universität München

Modeling Ternary Mixing in Turbulent Flow

Dipl.-Ing. Univ. Frank Victor Fischer

Technische Universität München
Institut für Energietechnik

Lehrstuhl für Thermodynamik

Modeling Ternary Mixing in Turbulent Flow

Dipl.-Ing. Univ. Frank Victor Fischer

Vollständiger Abdruck der von der Fakultät für Maschinenwesen der Technischen Universität München zur Erlangung des akademischen Grades eines

DOKTOR-INGENIEURS

genehmigten Dissertation.

Vorsitzende:
Univ.-Prof. Dr. rer. nat. Sonja Berensmeier
Prüfer der Dissertation:
1.Univ.-Prof. Wolfgang Polifke, Ph.D.
2.Univ.-Prof. Dr.-Ing. habil. Michael Manhart

Die Dissertation wurde am 27.06.2012 bei der Technischen Universität München eingereicht und durch die Fakultät für Maschinenwesen am16.01.2013 angenommen.

To my grandmother, who, at the age of 102, passed away during the last days of writing this thesis

Consider again that dot. That's here. That's home. That's us. On it everyone you love, everyone you know, everyone you ever heard of, every human being who ever was, lived out their lives. The aggregate of our joy and suffering, thousands of confident religions, ideologies, and economic doctrines, every hunter and forager, every hero and coward, every creator and destroyer of civilization, every king and peasant, every young couple in love, every mother and father, hopeful child, inventor and explorer, every teacher of morals, every corrupt politician, every "superstar", every "supreme leader", every saint and sinner in the history of our species lived there – on a mote of dust suspended in a sunbeam.

The earth is a very small stage in a vast cosmic arena. Think of the rivers of blood spilled by all those generals and emperors so that in glory and in triumph they could become the momentary masters of a fraction of a dot. Think of the endless cruelties visited by the inhabitants of one corner of the dot on scarcely distinguishable inhabitants of some other corner of the dot. How frequent their misunderstandings, how eager they are to kill one another, how fervent their hatreds.

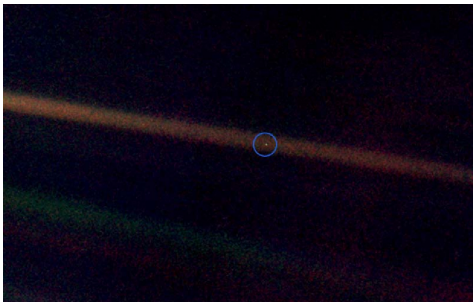

Earth, photographed by NASA's Voyager 1, from a distance of 6 billion kilometers

Our posturings, our imagined self-importance, the delusion that we have some privileged position in the universe, are challenged by this point of pale light. Our planet is a lonely speck in the great enveloping cosmic dark. In our obscurity – in all this vastness – there is no hint that help will come from elsewhere to save us from ourselves.

The Earth is the only world known so far to harbor life. There is nowhere else, at least in the near future, to which our species could migrate. Visit, yes. Settle, not yet. Like it or not, for the moment the Earth is where we make our stand.

It's been said that astronomy is a humbling and character-building experience. To my mind, there is perhaps no better demonstration of the folly of human conceits than this distant image of our tiny world. To me, it underscores our responsibility to deal more kindly and compassionately with one another and to preserve and cherish that pale blue dot, the only home we've ever known.

Carl Sagan, Pale Blue Dot: A Vision of the Human Future in Space

1 Acknowledgments

This work was created at the Lehrstuhl für Thermodynamik of the Technische Universität München, and was funded by the Deutsche Forschungsgesellschaft.

First and foremost I would like to thank my doctoral advisor,Univ.-Prof. Wolfgang Polifke, Ph.D. for his support and confidence. Also, for his personal interest he takes in his doctoral students and for his enthusiasm for turbulence modeling, which resulted in interesting and fruitful discussions. Finally, for the possibility to work autonomously, but then providing guidance where it was due. I am grateful thatUniv.-Prof. Dr.-Ing. habil. Michael Manhart found time to be an examiner for this thesis. For several years, we were working within the same SPP1141 striving for deeper understanding of mixing processes using numerical simulation. I would like to extend my thanks toUniv.-Prof. Dr. rer. nat. Sonja Berensmeier for taking the chair of the examination board.

I am thankful for the years I could spend with my colleagues at the department. They were a source of inspiration and their ideas for their own projects often resulted in deeper understanding of my own work. I also thank a number of undergraduate students with whom I worked, first and foremost Balaji Muralidharan, who completed his Master thesis under my supervision and supplied a large number of ideas to this project. Special thanks have to go to my cube mate Volker Kaufmann, with whom I have spent almost my entire time working at the university. We shared similar interests, faced similar problems and often found similar solutions. Without him, the time at the university would probably have been less productive and certainly less enjoyable.

I am truly grateful to my family and the many people that are my friends. Their continued support and guidance during these years have been crucial. I would like to especially thank my partner Alexandra for putting up with me even during the less enjoyable time during this work, which, I think, is a non-optional part of any scientific work. I wish her all the best for her own doctoral thesis. I thank countless teachers, professors and instructors with whom I had the pleasure of learning two and a half decades. They have sparked a flame of interest in science and technology which is inextinguishable.

Last but not least, I want to thank my current employer, TNG Technology Consulting GmbH, especially the current managing directors Henrik Klagges, Gerhard Müller and Christoph Stock, who allowed me to complete this thesis during my employment. Without their trust and support, this work might never have been completed.

Munich, June 2012 *Frank Victor Fischer*

Abstract

Thoroughly understanding mixing processes is crucial in order to assess the performance of a wide variety of chemical reaction systems, ranging from internal combustion engines to biochemical reactors. While the Direct Numerical Simulation, or DNS, is a numerical tool that provides deep insight into the phenomenon of turbulent mixing, the astronomical computational requirements of DNS are prohibitive for large scale technical application. In the present work, a model for Large-Eddy Simulation, or LES, was devised, which can accurately predict mixing processes by employing multiple, correlated mixture fractions. The input for the mixing models themselves are first and second order statistical moments of the distributions. Transport equations for these moments have been formulated, along with the models required for closure.
DNS and LES for a co-annular jet-in-crossflow configuration have been executed in order to assess the performance of the model. The quality indicator of the model performance is a reaction rate using an Arrhenius assumption. For the Reynolds numbers accessible by DNS, it is shown that the devised model predicts these reaction rates with high accuracy.

Contents

1 Acknowledgments vi

Nomenclature **xiii**

1 Introduction **1**
1.1 Modeling of Mixing Processes 1
1.1.1 Joint Presumed Discrete Distributions - a Novel Approach to Describing Mixing Processes 4
1.2 CFD Simulations using LES Modeling 6
1.3 Structure of the Thesis 8

2 Theory of Turbulent Flows **11**
2.1 Fundamentals of Fluid Mechanics 11
2.1.1 Equations of Conservation 11
2.1.1.1 Conservation of Mass 13
2.1.1.2 Conservation of Momentum 14
2.1.1.3 Conservation of Energy 15
2.1.1.4 Scalar Transport 16
2.1.2 Closure of the Conservation Equations 16
2.1.3 Simplifications for Incompressible Flows 18
2.2 Theory of turbulent flows 20
2.2.1 Definition of the Reynolds Number 22
2.2.2 Kolmogorov's Theory of Turbulence 23
2.3 Turbulent Mixing 25
2.3.1 Mixture Fractions, Mass Fractions and Molar Fractions . . 25
2.3.1.1 Mass Fraction 25
2.3.1.2 Mixture Fraction 26
2.3.2 Schmidt Number 26
2.4 Turbulent Reaction 27
2.4.1 Turbulent Damköhler Number 27
2.4.2 Reaction Rates 27
2.5 Computation of turbulent flows 28
2.5.1 DNS 28
2.5.1.1 DNS with Schmidt Number Around Unity . . . 28

2.5.1.2 Higher Schmidt Numbers in DNS 29
2.5.2 RANS 30
2.5.2.1 Turbulent Viscosity 31
2.5.2.2 Turbulence Models for RANS 31
2.5.3 LES 32
2.5.3.1 Filtering of the Navier-Stokes Equations 32
2.5.3.2 LES Models 35

3 Mixing Models **39**
3.1 Fundamentals of Mixing Models 39
3.2 Mechanical-to-Scalar Time Scale Ratio 40
3.3 Mixing Models 40
3.3.1 IEM / LMSE 41
3.3.2 Modified Curl 41
3.3.3 Mapping Closure 42
3.3.4 Euclidian Minimum Spanning Tree 42
3.3.5 PSP 42
3.4 A Biased, Multi-Variate Mixing Model 43
3.4.1 Variance Adjustment 45
3.4.2 Covariance 49

4 Probability Density Functions **55**
4.1 Closure for the Chemical Source Term 56
4.2 Flow Description Using PDFs 56
4.2.1 One-Point, Velocity PDF 57
4.2.2 One-Point Velocity Composition PDF 57
4.2.3 One-Point Composition PDF 57
4.2.4 One-Point Joint PDF 58
4.3 Filtered Density Functions 58
4.4 Different PDF Approaches 59
4.4.1 Presumed PDFs 59
4.4.2 Transported PDFs 60
4.5 Joint Presumed Discrete Distributions (jPDD) 61
4.6 Transport Equations for PDFs 62
4.6.1 Transport Equation for a Joint PDF 62
4.7 Transport Equations for Statistical Moments 63
4.7.1 Scalar Variance 63
4.7.2 Closure for the Scalar Dissipation Rate 64
4.7.3 Scalar Covariance 66

4.7.4 Closure for the Cross Dissipation Rate 66
4.7.5 The Full Set of Transport Equations 67

5 A Priori Validation of Model Assumptions 69
5.1 Validation Strategy 69
5.2 Validation Configuration 70
5.3 Solvers and Setup 71
5.3.1 MGLET 71
5.3.2 OpenFOAM 74
5.4 Post-processing of DNS Data 75
5.5 Post Processing Results 79
5.5.1 Variances and Scalar Dissipation Rates 79
5.5.2 Covariance and Scalar Cross Dissipation Rate 83
5.5.3 Mechanical to Scalar Time Scale Ratio 83
5.5.4 Transport equations 86
5.6 jPDDs and Reaction Rates 87
5.7 Additional Parameters 90

6 Conclusions and Outlook 93

Bibliography 97

List of Figures 103

A Derivation of the Covariance 107

B Quality of Mixing 109

C Implementation of the Transport Equations in OpenFOAM 111

Nomenclature

Latin Symbols

$\mathbf{c}$	Concentration vector
$\mathbf{f}$	Mixture fraction vector
$\overline{f'^2}$	Sub-grid scale scalar variance
$\overline{f_1' f_2'}$	Covariance of f_1 and f_2
c	Concentration
c_p	Specific heat at constant pressure
C_R	Modelling parameter for the timescale ratio
c_v	Specific heat at constant volume
e	Inner energy
f	Mixture fraction
$F_x(X;x,t)$	PDF of variable x at a point (x,t)
g_i	Volume force, e.g. gravity
H	Total enthalpy
h	Enthalpy
M	Molecular weight
n_i	Normal vector of a surface
p	Pressure
q_i	Heat flux vector
R	Ideal gas constant
r_{ij}	Rotation tensor
S	Surface
s	Entropy
s_{ij}	Deformation tensor
T	Temperature
u_i, u_j	Vector of velocity
V	Volume
w	Heat production
x_i	Spatial coordinate
y	Mass fraction

t	Time

Greek Symbols

Δ	Filter width
η	Kolmogorov lenth scale
Γ	Coefficient of diffusion
Γ	Coefficient of diffusion
Γ_{SGS}	Eddy diffusivity
κ	Wave number
μ	Dynamic viscosity
μ_d	Pressure viscosity
ν	Kinematic viscosity
ω	Reaction rate
$\overline{\chi}$	Scalar dissipation rate
$\overline{\varepsilon}$	Dissipation rate
$\overline{\kappa}$	Turbulent kinetic energy
Φ	Point in sample space of variable ϕ
ϕ	Passive scalar
ρ	Density
σ_i	Shear stress applied to a surface
τ	Turbulent or mechanical time scale
τ_η	Kolmogorov time scale
τ_ϕ	Scalar time scale
τ_f	Characteristic mixing time
τ_{ij}	Shear stress tensor

Superscript Indices

(i)	i-th particle
*	Dimensionless flow value

Dimensionless Quantities

Da_t	Turbulent Damköhler number
Re_η	Kolmogorov scale Reynolds number
Sc_{SGS}	Sub-grid scale Schmidt number
Da	Damköhler number
M,Ma	Mach number

Re	Reynolds number
Sc	Schmidt number

Acronyms

CFD	Computational Fluid Dynamics
DNS	Direct Numerical Simulation
FDF	Filtered Density Function
jPDD	Joint Presumed Discrete Distribution
LES	Large-Eddy Simulation
PDF	Probability Density Function
RANS	Reynolds-Averaged Navier-Stokes

1 Introduction

This research was performed at the Lehrstuhl für Thermodynamik, TU München in Germany, financed by the Deutsche Forschungsgesellschaft within the Schwerpunktprogramm SPP1141, running from 2003 to 2009. The objective of SPP1141 was to further the understanding of mixing processes on a theoretical level by combining experimental research with the development and application of computational methods. The aim of project PO710/4 of SPP1141, on which this thesis is based, was to develop and validate an LES model to simulate turbulent mixing of three streams, so called "ternary mixing" processes. Validation was planned within the SPP1141 versus both DNS data and experimental results. The method presented herein has previously been successfully applied in the Reynolds-Averaged Navier-Stokes (RANS) context by Brandt et al., 2003 and is now adapted for application in LES.

The initial problem setting was the SEV [1] burner of the Alstom GT26 stationary gas turbine (see figure 1.1 for a schematic). In this particular case, the hot exhaust from the high-pressure turbine is fed into a second burner, called the SEV, where additional fuel is consumed. In order for the fuel to not ignite right at the injection point due to the high temperatures of the first burner, it is shielded from the exhaust gases by a mantle of cooling air as schematically shown in figure 1.2. This configuration is an example of "ternary mixing", which occurs in a wide variety of technical applications.

1.1 Modeling of Mixing Processes

Mixing processes play a crucial role in understanding reactive systems, which occur both in nature and technical applications. As a chemical reaction can only take place when the reactants are in molecular contact so that the electron hulls of the atoms or molecules in question can interact, understanding the mixing process will enable assessing and optimizing the reaction system itself. In many cases,

1 The first burner is called the EV burner, for EnVironmental, while the second burner after the high pressure turbine is called SEV for Sequential EnVironmental.

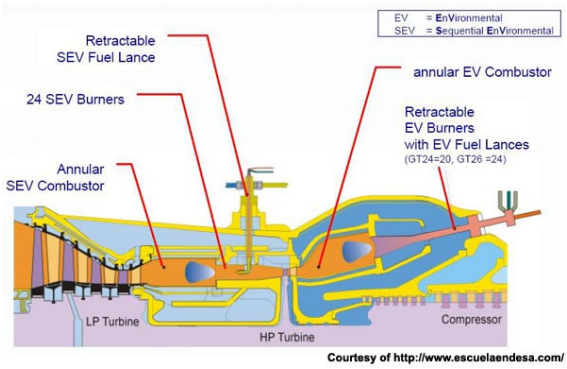

Figure 1.1: Schematic of the GT26 gas turbine, main flow is from right to left in this case

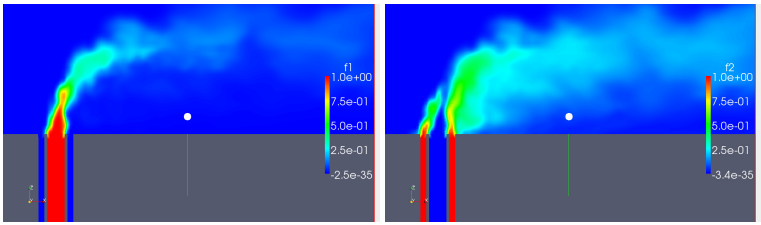

Figure 1.2: Schematic of a co-annular jet in cross flow. Main flow is from left to right. Left image displays the central jet, right image shows the annular jet

the mixing takes place in a turbulent regime, where a large number of eddies of various sizes exist throughout the flow field. The interaction between those eddies and the concentration fields of the flow largely determines the parameters of the mixing process, such as mixing quality and homogeneity. Within the SPP1141, it was noted that assessing the mixing quality itself is a challenging task. While beyond the scope of this thesis, a short overview of the findings can be found in appendix B.

Both turbulence and mixing are statistical processes. In this context variables are often decomposed into a mean variable and a fluctuation. As the reaction rate depends on the concentrations and the temperature in a highly non-linear fashion, the mean reaction rate of computational cell is not equal to the reaction rate of the mean values for concentrations and the temperature. In other words, in order to accurately compute the reaction rate, knowledge of the fluctuations of the variables is needed.

Methods using *probability density functions* or PDF methods lend themselves to describe such statistical processes. Here, a probability function determines the likelihood that a flow variable takes a certain value. One of the most successful group of methods for describing turbulent mixing processes are *Monte-Carlo based transported PDF* methods, where the mixing state of a computational cell is represented by a large number of mass-less particles within the cell, which are carrying properties that describe the mixing state. These particles are convected by the velocity field. For mixing on small scales, *mixing models* are employed, which describe the interaction (i.e. molecular mixing) of the particles. One of the advantages of this scheme is the intrinsic closure of the chemical source term. One simply has to sum up the reaction rate that the mixing state of each particle provides to obtain the reaction rate within the computational cell. Modeling the reaction rate is the prime reason why a precise description of the mixing state is required.

However, for this method to be statistically stable, each cell requires a large number of particles. This number then multiplies by the number of cells, yielding an enormous amount of particles, which often places transported PDF methods outside the realm of computational cost-effectiveness for technical applications.

1.1.1 Joint Presumed Discrete Distributions - a Novel Approach to Describing Mixing Processes

The present work attempts to model the unclosed terms of the sub-grid scale scalar unmixedness by using a novel approach. It combines the advantages of transported PDF and presumed PDF methods, which give the distribution a predetermined shape, characterized, for instance, by its moments. The model in this work approximates the sub-grid scale distribution (filtered density functions, FDFs) of the composition using particle ensembles. Mixing models, as known from transported PDF methods, are used to generate the distributions. However, in order to ease the computational cost of the simulation, the large number of particles within the domain are removed. In their stead, transport equations for the statistical moments of the distribution are solved. The mixing model then starts with a completely unmixed distribution and produces a distribution of given first and second order moments, which in turn are determined by the transport equations.

It has been shown that a distribution can be completely characterized by its (infinite) number of statistical moments. As this is impractical, only the first two moments are solved in this work using transport equations. Here, the first-order moments correspond to the means of the distribution, while the second-order moments are the variances and the covariances of the distribution. As particles can convey an arbitrary number of properties, this approach lends itself well to systems that need multiple mixture fractions for representation. These multi-variate distributions are then referred to as *joint presumed discrete distributions* or *jPDD*. These distributions are characterized using their first and second order moments, which represent the means and variances of the distribution. If the distribution contains values for multiple mixture fractions, the second order moments do not only represent the variance of any of the mixture fractions, but also the co-variances or correlations between those fractions. As such, a derivation of a transport equation for the co-variance is needed, which then contains the unclosed term of the *scalar cross-dissipation rate*. Transport equations for these moments are used that do not assume any equilibrium between the production and dissipation of sub-grid scalar variance. Thus, models for the sub-grid *scalar dissipation rate* and the above-mentioned scalar cross dissipation rate have to be employed, unless one wants to go the extra mile of deriving a separate transport equation for this quantity, which would lead to yet another set of unclosed terms, which would give rise to new modeling problems [Fox03]. Hence, the new computational procedure developed in this thesis is as follows (see also figure 1.3 for a graphical representation).

1. Before the actual simulation, in a preprocessing step (right side):

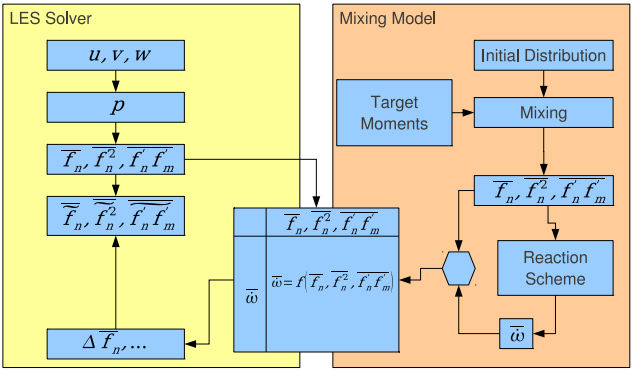

Figure 1.3: Work flow diagram of the basic idea in this thesis

a) The mixing model generates distributions, starting from initial distributions, which cover the whole required parameter space

b) A reaction scheme is applied to these distributions, obtaining a reaction rate that corresponds to each set of moments

c) The reaction rate is placed into a table, with the moments as parameters.

2. During the simulation (left side), the solver performs the following steps:

a) Compute flow variables (pressure, density and temperature if needed)

b) Solve the transport equations for the statistical moments

c) Extract the reaction rate that corresponds to the moments found in the cell from the table

d) Adjust all variables that are influenced by the reaction rate

As the table only contains the statistical moments as parameters, it can be reused for different simulations, provided these employ the same reactive systems.

In order not to populate large parts of the table that will never be used in a computation, the table can as well be populated *in situ*. In this scheme, when the simulation commences, all cells of the table are empty and the corresponding reaction rate of a cell will be computed on first use, which is a time-consuming computation. All subsequent accesses to the same cell of the table then reduce to a simple look-up.

It can therefore be assumed that this approach will be slightly less accurate than traditional transported PDF methods, albeit at considerably reduced computational effort. This will enable this new method to provide computational solutions to problems of applied interest. It is also expected to produce more reliable results than existing presumed PDF methods.

1.2 CFD Simulations using LES Modeling

Computational Fluid Dynamics, or CFD, are becoming a more and more important tool for engineers and scientists. CFD is used not only for the design of technical applications but also for the study of natural phenomena ranging from climate simulations down to flow simulations of the blood in organisms. Three major factors contribute to this development.

First of all, both the computational resources and the available memory in today's computers (ranging from notebooks to supercomputers) continue to grow at an exponential pace. Thus it is possible to compute more complex problems with fewer simplifications as well as make parametric studies with a large number of parameters. Meuer [Meu08] shows that since 1993, the pure computational power of the fastest supercomputers in the world has grown by a factor of almost 20000 and the computational power of the largest supercomputers at a certain point in time is available in notebooks approximately 18 years later. This allows, on the one hand, to perform more and more computationally challenging simulations on very large computers while simpler simulations can today be performed with very limited effort from a computing point of view, compared to what was necessary only a few years ago.

A second point why CFD is more widely used is the fact that for optimization processes or parametric studies, it is both costly and complex to construct a vast number of prototypes that are needed to perform experiments on. While the fully automatic optimization of flow systems using, for instance, genetic algorithms is

still in its infancy, it is apparent that modifying the geometric or flow parameters in a simulation most often requires much less time and effort compared to an experimental setup that would have to be modified over and over.

The third factor is that CFD allows access to any physical parameter at any given space-time coordinate within the computational domain. Experimental setups are usually limited in the number of parameters they can determine at a given time and can usually only obtain measurements for a limited geometrical region.

However, as shown in detail later, simulating all scales of turbulent phenomena in large technical flow systems, like airborne or stationary gas turbines, remains a formidable or, in many cases today, an impossible task. As the flow is described using non-linear partial differential equations, for which no general analytical solutions are known[2] , numerical solution methods need to be applied. As turbulence is an inherently three-dimensional phenomenon, the entire domain that is to be simulated needs to be divided into a large number of domains in each physical dimension, typically referred to as *computational cells*. Also turbulence has transient properties that require the computation to run over a large number of (typically very small) time steps.

Whenever all scales of the turbulence are simulated directly, the method is referred to as *Direct Numerical Simulation* or *DNS*. While this is from a physical point of view the least challenging and most desirable method, its use is limited using current-generation computers.

In order to keep the computational effort of the simulation at bay, the number of cells needs to be reduced, which is the main goal of the *Large-Eddy-Simulation* or *LES*. It is generally assumed that the geometry of a flow system affects large scale of the turbulence, while the smaller scales are more homogeneous and isotropic in nature. LES makes use of this fact: Large scales, which are not only more geometry-dependent but also carry most of the turbulent energy, are resolved by the grid (i.e. simulated directly), while the smaller scales (carrying less energy and being more isotropic) are modeled by one of the many available approaches mentioned in chapter 2.

As such the LES is more flexible in approach than the computationally least expensive method: The *Reynolds-Averaged Navier-Stokes* or *RANS* simulations. In RANS, only the mean flow field is computed directly, and all scales of turbulence

2 Note that there are several academic corner-cases where an analytical solution to the describing equations exist. While those cases are of no importance for technical applications, they remain an important tool of validating the solvers of such differential equation systems.

are modeled. While this reduces the number of cells that are required for any given configuration, it places a very heavy burden on turbulence modeling. Any model used in RANS requires not only the correct display of the small, isotropic scales (like in LES), but also needs to model non-isotropic turbulent structures induced by the geometric configuration of the flow. It is apparent that the applicability of RANS is limited if the model cannot capture the turbulence correctly.

1.3 Structure of the Thesis

The first part of the thesis, chapter 2, presents the fundamentals required to describe turbulent mixing and will also show an introduction to reactive systems. After deriving the fundamental Navier-Stokes equations, which can be used to describe single phase turbulent flows in almost any case, the phenomenon of turbulence, which is a result of the nonlinearity of the Navier-Stokes equations, is explained. Then methods that describe the chemical state of a computational cell are shown. A final section of this chapter will present and discuss the previously mentioned computational methods (RANS, LES and DNS) to solve the Navier-Stokes Equations. Some standard models that are used for LES approaches will be shown as well.

In the second part, chapter 3, will then outline the mixing model that has been developed in the course of this thesis. Since FDFs can be represented by ensembles of particles without complex analytical descriptions, ensembles with predetermined first and second order moments are generated using mixing models. This is done by starting from a state of maximum unmixedness for a given set of means. First, the fundamentals of mixing models are discussed, then specific models taken from literature and the required changes for ternary mixing are shown.

Chapter 4 will cover *probability density function* or *PDF* methods. These methods are used to describe the state of a specific random variable within a cell. It will be seen in the chapter that a PDF can not only be an analytical function (i.e. described by a formula) but can also be represented by a statistically significant number of particles (i.e. described by an ensemble). As PDF methods have been developed for the RANS context, some differences to the LES implementation will be described. In LES, density functions usually describe the unresolved state of a filtered variable and are hence called *Filtered Density Functions* or *FDFs*. As the mixing model needs statistical moments of the distributions that are to be generated, transport equations for those moments are derived. Also, it is shown

that filtering these transport equations for LES yields unclosed terms. Models and methods for closing these terms are also displayed.

Chapter 5 then shows the validation of the model versus DNS data. One part of that chapter shall describe the numerical setup and data handling of the DNS data, while the second part compares the model and DNS data directly, while 6 will give a short summary, conclusion and ideas for future projects that can build upon this work.

2 Theory of Turbulent Flows

This chapter shall summarize the theory of turbulent flows. Before the concept of *Large-Eddy-Simulation* is introduced, the fundamental laws which lead to the *Navier-Stokes equations* are presented in section 2.1. The phenomenon and theory of turbulence is covered in section 2.2. Section 2.3 then explains the basics of turbulent mixing and introduces the concept of mixture and mass fractions to simulate multi-species flows. The next section of this chapter, 2.4, then gives an overview of turbulent reacting flows and the closure of the reaction term, while the final section 2.5 then shows the three different strategies that exist for solving fluid phenomena.

2.1 Fundamentals of Fluid Mechanics

Throughout this thesis, single-phase mixtures of gas fluids are used. This first section derives the fundamental laws to describe such flows.

2.1.1 Equations of Conservation

Deriving the governing equations for single phase fluids commences by using the fundamental conservation laws. There are a number of *exact* conservation laws, three of which are required here for the derivation:

- Conservation of mass-energy. As no nuclear reactions are present, the *approximate* conservation laws of mass and energy can be regarded separately
- Conservation of linear momentum
- Conservation of angular momentum

Using these laws, a first set of equations is obtained, which possesses more unknowns than equations. The subsequent sections then introduce the additional laws required for the closure of the set. The conservation laws are set up on a volume element as depicted in figure 2.1.

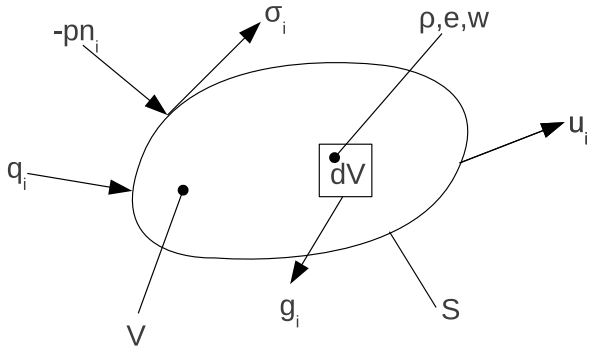

Figure 2.1: Volume element of a fluid with the required physical quantities to describe the flow
V: volume of the element
S: surface of the element
ρ: density
e: internal energy
w: heat production
σ_i: shear stress
p: pressure
n_i: normal vector
q_i: heat flux vector
u_i: velocity vector
g_i: volume force

2.1.1.1 Conservation of Mass

The conservation of mass states that the mass of a volume of material remains constant, thus, in integral form

$$\frac{d}{dt}\int_V \rho d\overline{V} = 0. \tag{2.1}$$

If Reynolds' Transport Theorem [Lea07]

$$\frac{d}{dt}\int_V \Psi(x_i,t)d\overline{V} = \int_V \frac{\partial \Psi(x_i,t)}{\partial t}d\overline{V} + \oint_S \Psi(x_i,t)\frac{dx_i}{dt}\cdot d\overline{S} \tag{2.2}$$

and the Divergence Theorem [MV89]

$$\int_V \frac{d\Psi_i}{dx_i}d\overline{V} = \int_S \Psi \cdot n_i d\overline{S}, \tag{2.3}$$

with Ψ being an arbitrary property of the flow, are applied to equation (2.1), the integral form of the conservation of mass takes the form of

$$\frac{d}{dt}\int_V \rho d\overline{V} = \int_V \left(\frac{\partial \rho}{\partial t} + \frac{\partial \rho u_i}{\partial x_j}\right) d\overline{V} = 0. \tag{2.4}$$

Here, u_i is the velocity of the fluid in all three spacial dimensions.

As equation (2.4) must be satisfied for all volumes, the integrand $\left(\frac{\partial \rho}{\partial t} + \frac{\partial \rho u_i}{\partial x_j}\right)$ needs to be zero in all cases, yielding the conservation law of mass in differential form

$$\frac{\partial \rho}{\partial t} + \frac{\partial \rho u_i}{\partial x_i} = 0. \tag{2.5}$$

This *Eulerian form* of the equation is based on the *control volume* scheme. A second form, called *the convective form* or *Lagrangian form* tracks units of fluids along their paths of moments. As most CFD codes employ the control volume approach, only that will be used throughout this thesis.

2.1.1.2 Conservation of Momentum

According to Newton's second law of motion, the change of momentum of a control volume equals the sum of all applied forces [Bat67]

$$\frac{d}{dt}\int_V \rho u_i d\overline{V} = \oint_S (-pn_i + \sigma_i)\, d\overline{S} + \int_V \rho g_i d\overline{V}. \tag{2.6}$$

The right hand side of equation (2.6) contains three kinds of forces, the surface forces in the first integral, and the volumetric forces in the second integral:

- g_i is the change in momentum due to volumetric forces like gravitation or electromagnetic forces. These forces are disregarded in the rest of this thesis as their influence on the flow is negligible.
- pn_i is the pressure on the control volume, i.e. a force perpendicular to its surface.
- σ_i are the stresses tangential to its surface, which result from the viscosity, as will be shown in section 2.1.2.

With the identity

$$\tau_{ij} n_j = \sigma_i, \tag{2.7}$$

and using the same laws as for the conservation of mass on equation (2.6) gives the differential form of the momentum equation

$$\rho \frac{Du_i}{Dt} = -\frac{\partial p}{\partial x_i} + \frac{\partial \tau_{ij}}{\partial x_j} + g_i, \tag{2.8}$$

with the operator $\frac{D}{Dt} = \frac{\partial}{\partial t} + u_i \frac{\partial}{\partial x_j}$.

The conservation of angular momentum requires that the tensor τ_{ij} is symmetric, thus

$$\tau_{ij} = \tau_{ji}. \tag{2.9}$$

Here, equation (2.8) represents actually three individual equations, one for each spatial direction.

2.1.1.3 Conservation of Energy

To complete the set of Navier-Stokes equations, the conservation of energy has to be taken into account. As demanded by the first law of thermodynamics, the sum of energy within a control volume, which itself is the sum of volume specific internal energy e and kinetic energy $\frac{1}{2}u_i u_i$, equals the power induced by the forces plus the heat transfer into the volume, and the heat produced within the volume itself. This gives, in integral form

$$\frac{d}{dt}\int_V \rho\left(e+\frac{1}{2}u_i u_i\right)d\overline{V} = \oint_S (\sigma_i - p n_i)\,u_i - q_i n_i d\overline{S} + \int_V \rho\,(g_i u_i + w)\,d\overline{V}. \quad (2.10)$$

Where q_i is the heat flux vector of the control volume and w is the heat production by a chemical or nuclear reaction or absorption of radiation.

Again, this can be brought into differential form, yielding

$$\rho\frac{D}{Dt}\left(e+\frac{1}{2}u_i u_i\right) = \frac{\partial}{\partial x_j}\left(\tau_{ij}u_i - p u_j - q_i\right) + \rho g_i u_i. \quad (2.11)$$

Here, the heat production w can be either heat production by an ongoing reaction in the fluid or the radiation balance, or a combination thereof. For this thesis, both the radiation (either emitted or absorbed) and the heat production/consumption by a chemical reaction are neglected, thus $w = 0$ at all times. Also, body forces like gravitation or electromagnetism are not taken into account, thus $g_i = 0$.

In open systems, where there is influx or outflux of fluid, it has been proven more productive to replace the specific internal energy e with the enthalpy h or the total enthalpy H. The relation between e, h and H is:

$$h = \frac{p}{\rho} + e, \quad (2.12)$$

$$H = h + \frac{u^2}{2}. \quad (2.13)$$

Using this and equation (2.11), including $w = 0$ and $g_i = 0$, the conservation of energy can be rewritten as the conservation of total enthalpy

$$\rho\frac{DH}{Dt} = \frac{\partial p}{\partial t} + \frac{\partial u_i \tau_{ij}}{\partial x_j} - \frac{\partial q_j}{\partial x_j}. \quad (2.14)$$

2.1.1.4 Scalar Transport

The general transport equation for a passive scalar ϕ reads [Fox03]

$$\frac{D\phi}{Dt} = \frac{\partial}{\partial x_i}\Gamma_\phi \frac{\partial \phi}{\partial x_i} + S_\phi. \tag{2.15}$$

The left hand side contains the time derivative and the standard convection term of a property that is propagated with the flow velocity, while on the right hand side, there is the diffusive time with a generic diffusivity Γ_ϕ, and a generic source term S_ϕ. If a conserved scalar (i.e. no sources) and a constant diffusivity is present, equation (2.15) simplifies to

$$\frac{D\phi}{Dt} = \Gamma \frac{\partial^2 \phi}{\partial x_i^2}, \tag{2.16}$$

which is the form that is used in this work for mixture fractions, since they do not have source terms as explained in chapter 3.

It is important to note that the value ϕ does not occur in equation (2.8) or equation (2.4), making the scalar passive. As such, the flow field can be solved independently from the scalar field(s).

2.1.2 Closure of the Conservation Equations

Equation (2.5), (2.8) and (2.14) are 5 equations[1], but the system contains 15 unknowns: ρ, u_i (three unknowns), p, τ_{ij} (six), H and q_i (three). Hence, additional equations are needed to close the system of equations. Due to the pressures and temperatures (around standard conditions) that are present throughout this work, it is possible to use the *ideal gas law* to state a relationship between pressure, density and temperature [Gri77] as

$$p = \rho RT. \tag{2.17}$$

The thermodynamic equations of state yield the relation between the internal energy and the temperature as

1 note that equation (2.8) displays three equations

$$de = c_v dT, \tag{2.18}$$

where c_v is the specific heat at constant volume.

The tensor of velocity gradients can be split into a symmetric and an antisymmetric part

$$\frac{\partial u_i}{\partial x_j} = \frac{1}{2}\left(\frac{\partial u_i}{\partial x_j} + \frac{\partial u_j}{\partial x_i}\right) + \frac{1}{2}\left(\frac{\partial u_i}{\partial x_j} - \frac{\partial u_j}{\partial x_i}\right) = s_{ij} + r_{ij}. \tag{2.19}$$

The symmetric part s_{ij} is the *deformation tensor* while the antisymmetric part r_{ij} is the *rotation tensor*. The trace of the deformation tensor is the volume dilatation rate, the elements of the trace are the extension rates in the spatial dimensions.

A law for the shear stress tensor τ_{ij} can be obtained using kinetic gas theory. There, the Enskog-Chapman method assumes that only small deviations from the local thermodynamic equilibrium exist, which is a valid assumption for a very large range of flow phenomena[2] [Fri01]. The shear stress tensor that can be derived is then

$$\tau_{ij} = 2\mu s_{ij} + \left(\mu_d - \frac{2}{3}\mu\right) s_{kk}\delta_{ij}, \tag{2.20}$$

where μ is the (dynamic or absolute) viscosity of the fluid and μ_d is its pressure viscosity. The viscosity itself is a function of the temperature of the fluid, which can be approximated, for instance, by Sutherland's law. For cold flows, i.e. with very small or no temperature changes, it is assumed to be constant within the entire domain. The pressure viscosity is a result of the internal degrees of freedom of the gas molecules. Thus, it is exactly zero for monatomic gases. More generally $\mu_d = 0$ is assumed for most CFD applications, but the term plays a noticeable role in the dissipation of shock waves or ultrasonic waves [Fri02].

The same theory also derives a simple law, known as Fourier's law, for the heat flux q_i as

$$q_i = -\lambda \frac{\partial T}{\partial x_i}, \tag{2.21}$$

with λ as the thermal conductivity of the medium, which is assumed to be isotropic. Thus the heat transfer through the fluid is proportional to the negative temperature gradient within the fluid.

2 Typically, flow systems where this assumption is not valid, cannot be described using the Navier-Stokes equations. These include flows where the Knudsen number is low, like capillary flows or atmospheric reentry conditions

2.1.3 Simplifications for Incompressible Flows

In an incompressible flow the changes of density along the streamlines (i.e. paths of motion of a fluid particle) can be neglected, so

$$\frac{\partial \rho}{\partial t} + u_j \frac{\partial \rho}{\partial x_j} = 0. \tag{2.22}$$

With equation (2.22), the continuity equation (2.5) reduces to

$$\frac{\partial u_i}{\partial x_i} = 0. \tag{2.23}$$

In other words, incompressible flows possess no divergence in the velocity field. The incompressible version of the continuity equation no longer has a time derivative, which has large implications for the solution method compared to compressible flows. While in compressible flows, a time step operation is applied to both the momentum and continuity equations (disregarding the energy equation for this simplification), incompressible solvers can only perform a time stamp operation on the momentum equation and then have to correct the solution to a divergence-free one, which is usually performed using an iterative scheme.

While equation (2.23) is certainly satisfied for constant density flows, there are other configurations where incompressibility can be obtained.

In order to determine under which circumstances the compressibility of a fluid can be neglected, the total differential of the pressure

$$dp = \left(\frac{\partial p}{\partial \rho}\right)_s d\rho + \left(\frac{\partial p}{\partial s}\right)_\rho ds \tag{2.24}$$

has to be regarded. With the first differential being the speed of sound $a = \left(\frac{\partial p}{\partial \rho}\right)_s$ and the second differential defined as $\left(\frac{\partial p}{\partial s}\right)_\rho = \frac{\rho a^2}{c_p}\beta T$ and for thermic ideal gases $\beta = \frac{1}{T}$, equation (2.24) becomes, for a moving fluid particle

$$\frac{Dp}{Dt} = a^2 \frac{D\rho}{Dt} + \frac{\rho a^2}{c_p}\frac{Ds}{Dt}. \tag{2.25}$$

With the continuity equation in the form $\frac{1}{\rho}\frac{D\rho}{Dt} + \frac{\partial u_i}{\partial x_i} = 0$, equation (2.25) can be used to derive the amount of velocity divergence as

$$\frac{\partial u_i}{\partial x_i} = \frac{1}{\rho a^2}\left(-\frac{\partial p}{\partial t} - u_i \frac{\partial p}{\partial x_i}\right) + \frac{1}{c_p}\frac{Ds}{Dt}. \tag{2.26}$$

Applying the momentum equation and the entropy transport equation to this, gives the equation for the compressibility in dimensionless form

$$\begin{aligned}
\frac{\partial u_j^*}{\partial x_j^*} &= \frac{La_0^2}{a_0 t_0 a^2}\left(\frac{M_0}{2}\frac{\partial u_i^* u_i^*}{\partial t} - \frac{\rho_0}{\rho}\frac{\partial p^*}{\partial t*}\right) && (2.27)\\
&+ \frac{a_0^2}{a^2}\left(M_0^2 u_j^* \frac{\partial}{\partial x_j^*}\left(\frac{1}{2}u_i^* u_i^*\right)\right) && (2.28)\\
&- \frac{a_0^2}{a^2} u_i^* g_i && (2.29)\\
&- \frac{M_0^2}{Re_0}\frac{\rho_0 a_0^2}{\rho a^2}\left(u_i^* \frac{\partial}{\partial x_j^*} u_i^* x_j + \frac{1}{3} u_j^* \frac{\partial s_{ii}^*}{\partial x_j^*}\right) && (2.30)\\
&+ \frac{1}{Re_0}\frac{\rho_0 a_0^2}{\rho a^2}\left(\frac{1}{Pr}\frac{\partial}{\partial x_j^*}\frac{\partial T^*}{\partial x_j^*} + (\kappa - 1) M_0^2 \tau_{ij}^* s_{ij}^*\right). && (2.31)
\end{aligned}$$

The previous equation contains five different groups of terms

- The terms in the first line (2.27) are only of interest, if $\frac{L}{a_0 t_0}$ is at least of $O(1)$, i.e. high frequency or *acoustic* effects.
- The terms in the second line (2.28) are of convective nature and contain the term M_0^2. Thus, these terms are only of interest with respect to compressibility if the Mach number is large enough. Typically a limit of 0.2 or 0.3 is used for these effects.
- The third line (2.29) contains the volumetric forces. If the main volumetric force is gravity, this term is only significant if the size of the domain (in the direction of gravitation) is around the scale height. For air in Earth's gravity field, this value is in the order of 10km. For fluids where magnetic or electric forces are present, this term has to be regarded separately, for example in plasma flows.
- The forth term (2.30) represents viscous effects on the divergence of the flow field and contains the term $\frac{M_0^2}{Re}$. As the Navier-Stokes equation set is only valid if $Ma \ll Re$ [Fri01], these terms are very small and can be neglected.

- The final line (2.31) contains effects of dissipative nature and heat production. Here, the term $\frac{1}{Re}$ is present, which means these effects are only of interest if the temperature gradients are very steep.

In conclusion, low Mach number (below 0.2 or 0.3) flows where acoustic effects are not under consideration, or atmospheric flows with large vertical distances can generally be considered incompressible, i.e. $\frac{\partial u_i}{\partial x_i} = 0$.

2.2 Theory of turbulent flows

While the previous section explained the basic equations that govern the flows of fluids, the current one explains the phenomenon of turbulence and its implications. In general, flows exist in two major regimes, laminar and turbulent. A laminar flow exists when the flow regime can be divided into moving planes, with no mass exchange between the planes outside of molecular diffusion. In a turbulent flow, there is convection of mass perpendicular to the stream lines. This convection is generally chaotic in nature and can as such not be exactly predicted. This convection happens on a wide range of length scales ranging from typical geometric parameters of the flow down to the Kolmogorov scale, see also section 2.2.2.

Generally, the velocity field of the flow can be divided into two parts, a mean part and a fluctuation. The mean part is the result of arithmetically averaging the velocity over a large number of flow realizations at a given point in the computational domain, thus the mean flow is dependent only on the position [Dur07]. The decomposition then is

$$u_i(x_i,t) = \overline{u_i(x_i)} + u_i'(x_i,t), \tag{2.32}$$

$$\overline{u_i'(x_i,t)} = 0, \tag{2.33}$$

$$\overline{u_i'u_j'} \neq 0. \tag{2.34}$$

Equation (2.34) is of particular interest. While the mean of the fluctuations of a single dimension u_i is always zero (see equation (2.33)), the Navier-Stokes equations contain correlation terms like u_iu_j. The fluctuations of those terms do not cancel out. If the equations are filtered or averaged (explained in section 2.5), modeling these fluctuations becomes the crucial part of the solution.

The *turbulent kinetic energy* can be derived as

$$k \equiv \frac{1}{2}\overline{u_i'u_i'}. \tag{2.35}$$

Figure 2.2: Turbulent flow of exhaust and cooling gases during Space Shuttle mission STS-1 launch. Picture courtesy of NASA

Finally, the mean turbulent fluctuation u' can be computed from the turbulent kinetic energy as

$$u' = \sqrt{\frac{2}{3}k}. \tag{2.36}$$

As shown by Friedrich [Fri02], a transport equation for the vorticity can be derived by applying the rotation operator $\varepsilon_{ijk}\frac{\partial}{\partial x_j}$ to the momentum equation, which eventually results in

$$\frac{D\omega_i}{Dt} = \omega_j\frac{\partial u_i}{\partial x_j} - \omega_i\frac{\partial u_i}{\partial x_j} - \varepsilon_{ijk}\left(\frac{1}{\rho^2}\frac{\partial p}{\partial x_j}\frac{\partial \rho}{\partial x_k} - \frac{\partial}{\partial x_j}\left(\frac{1}{\rho}\frac{\partial \tau_{kl}}{\partial x_k}\right)\right), \tag{2.37}$$

or, if constant density of the flow is assumed [Fri03],

$$\frac{D\omega_i}{Dt} = \omega_j\frac{\partial u_i}{\partial x_j} + \frac{1}{\rho}\varepsilon_{ijk}\frac{\partial}{\partial x_j}\frac{\partial \tau_{kl}}{\partial x_k} = \omega_j\frac{\partial u_i}{\partial x_j} + \nu\frac{\partial}{\partial x_j}\frac{\partial \omega_k}{\partial x_j}. \tag{2.38}$$

The first term of the right hand side couples the vorticity with the velocity of the flow field. Equation (2.37) also shows that turbulence itself is an *inherently three-dimensional process*.

2.2.1 Definition of the Reynolds Number

The Reynolds Number gives the ratio of inertial forces to viscous forces in a fluid. This can be derived by using the time scale of the diffusion of momentum $t_{\text{diffusion}} = \frac{L^2}{\nu}$ and the time scale of convection of momentum $t_{\text{convection}} = \frac{L}{U}$. Here, L represents a characteristic length of the phenomenon (like the diameter of a pipe, the length of an airfoil, etc.) and U a characteristic velocity (for example the free-flow velocity or a the maximum velocity in a pipe). Thus, the Reynolds number becomes

$$Re = \frac{UL}{\nu}. \tag{2.39}$$

This number has a fundamental impact on the nature of the flow. This can be seen if equation (2.8) is made dimensionless using the following definitions, with values with an asterisk being the non-dimensional values and capitals for the reference values

$$u_i^* = \frac{u_i}{U}, \tag{2.40}$$

$$x_i^* = \frac{x_i}{L}, \tag{2.41}$$

$$t^* = t\frac{U}{L}, \tag{2.42}$$

$$p^* = \frac{p}{\rho U^2}, \tag{2.43}$$

it yields, if volumetric forces are disregarded,

$$\frac{\partial u_i^*}{\partial t^*} + u_j^* \frac{\partial u_i^*}{\partial x_j^*} = -\frac{\partial p^*}{\partial x_i^*} + \frac{\nu}{UL}\frac{\partial}{\partial x_j^*}\frac{\partial u_i^*}{\partial x_j^*} = -\frac{\partial p^*}{\partial x_i^*} + \frac{1}{Re}\frac{\partial}{\partial x_j^*}\frac{\partial u_i^*}{\partial x_j^*}. \tag{2.44}$$

Equation (2.44) contains the Reynolds number only in the last term of the right hand side, which leads to the following conclusions:

- Viscous phenomena become irrelevant in very high Reynolds number flows.
- Flows which have similar Reynolds numbers exhibit a similar behavior, when made dimensionless as above.

The Reynolds number also defines whether a flow is laminar or turbulent in nature.

2.2.2 Kolmogorov's Theory of Turbulence

Komolgorov [Kol41, Kol62] has shown that for homogeneous and isotropic turbulence, there is an energy cascade that transfers energy from the largest to the smallest eddies, if the production and dissipation of turbulent kinetic energy is in balance. The energy spectrum of turbulence has three ranges according to Pope, Tennekes and Lumley [Pop00, TL87].

- The *energy carrying range* or *large scale spectrum* which contains the largest eddies. Here, energy is transferred from the average flow into the turbulent scales. The mean flow, and hence the geometry, is paramount for this range.
- The *inertial range* is the range where energy is transferred from large eddies to smaller and smaller eddies, this transfer happens with a dissipation rate of
$$E(\kappa) = C_1 \kappa^{-\frac{5}{3}} \varepsilon^{\frac{2}{3}}. \tag{2.45}$$
Here, κ is the wave number of the eddies. ε is the *turbulent dissipation rate*, defined as
$$\varepsilon = C_2 \frac{u(r)^3}{r}, \tag{2.46}$$
with $u(r)$ as the fluid velocity in the eddy and the r as the size class (radius) of the eddy.
- The *dissipation range* is where the small eddies are dissipated by the viscosity of the fluid.

Within those ranges, four important length scales exist. In descending order of length, these are

- The *integral length scale*, defined as the mean size of the eddies, divided by the total energy in the eddies [Dur07]
$$l_t \equiv \frac{\int_0^\infty \frac{1}{\kappa} E(\kappa) d\kappa}{\int_0^\infty E(\kappa) d\kappa}. \tag{2.47}$$
The Reynold number based on the mean fluctuation and the integral length scale is called the *turbulent Reynolds number*
$$Re_t = \frac{u' l_t}{\nu}. \tag{2.48}$$

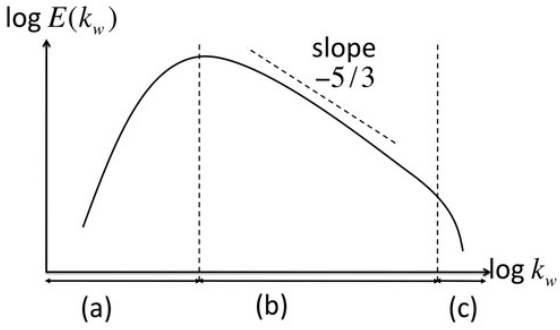

Figure 2.3: The turbulent energy cascade

This Reynolds number is often used for LES modeling, since it represents the ratio between turbulent diffusion and molecular diffusion, i.e. high turbulent Reynolds numbers imply that molecular diffusion effects can be neglected.

- The inertial length scale is the size that has the maximum turbulent kinetic energy, i.e. the separation of ranges (a) and (b) in figure 2.3.
- The Taylor length scale l_λ is the ratio between the mean fluctuation and the mean strain rate [Tay35]

$$l_\lambda \equiv \sqrt{\frac{u_i}{\frac{\partial u}{\partial x}}} = Re_t^{-\frac{1}{2}} l_t. \tag{2.49}$$

- The Kolmogorov length scale η represents a lower limit for the size of eddies, and has a time scale τ_η associated with it. Those, and the Kolmogorov Reynolds numbers are defined as

$$\eta = \left(\frac{\nu^3}{\varepsilon}\right)^{\frac{1}{4}}, \tag{2.50}$$

$$\tau_\eta = \left(\frac{\nu}{\varepsilon}\right)^{\frac{1}{2}}, \tag{2.51}$$

$$\mathrm{Re}_\eta = 1. \tag{2.52}$$

This Reynolds number is the ratio between turbulent diffusion and the molecular dissipation, thus this length scale is the lower size limit of the eddies.

2.3 Turbulent Mixing

All equations presented in this chapter up to now have been used to describe the flow of a single gas or mixture of gases. If mixing processes are to be described, additional information which describes the *mixing state*, i.e. the chemical composition of the fluid, is required.

2.3.1 Mixture Fractions, Mass Fractions and Molar Fractions

In order to describe mixing processes, the mixing state in a control volume needs to be described. Several definitions of such fractions exist which can be used for this purpose.

2.3.1.1 Mass Fraction

The most simple description of the mixing state is the mass fraction. It describes the presence of a species i by setting its mass m_i in relation to the mass in the whole control volume $dm = \rho dv$, where the density is the local density in the control volume, thus

$$Y_i = \frac{m_i}{m}. \tag{2.53}$$

As such, the sum of all mass fractions has to add up to unity

$$\sum_{i=1}^{n} Y_i = 1. \tag{2.54}$$

A transport equation for mass fractions of species i will have a chemical source term if a chemical reaction takes place within the fluid, where the species i is either produced or consumed.

2.3.1.2 Mixture Fraction

As shown previously, the chemical source term in the transport equation is the main source of closure problems when modeling turbulent reacting flows.

Starting from the mass fraction describes previously, the molar concentration c_i of a species i is defined as

$$c_i = Y_i \frac{\rho}{M_i}, \tag{2.55}$$

with ρ as the density of the mixture and M_i as the molecular weight of species i. Since in a reactive scheme multiple species exist, all concentrations make up the concentration vector $\mathbf{c}$.

Fox [Fox03] shows that in non-premixed cases, the concentration vector can be transformed into a mixture fraction vector $\mathbf{f}$ and a *reaction progress vector*. In this decomposition, the reaction progress vector is always zero at all inlet conditions. At high Reynolds numbers, the scalar fields of the mixture fractions are not determined by molecular diffusion, thus the transport equation of the mixture fractions is independent of the molecular properties of the species that constitute the flow.

Hence, the mixture fraction approach "marks" each influx boundary condition with an own mixture fraction f_i which follow the simple transport equation

$$\frac{Df_i}{Dt} = \Gamma \frac{\partial^2 f_i}{\partial x_i^2}, \tag{2.56}$$

with Γ as a general diffiusity for all the scalars. The reaction itself is then described by the transport equation of the reaction progress vector, which contains the transformed chemical source terms.

2.3.2 Schmidt Number

The Schmidt Number is defined as

$$Sc = \frac{\nu}{\Gamma}, \tag{2.57}$$

with Γ as the diffusivity of the scalar. Using this, the length scales of turbulent mixing are the Kolmogorov length scales and the *Batchelor length scale* l_B. The relation is defined as [Bat59]

$$l_n = \sqrt{Sc} l_\nu. \tag{2.58}$$

It shows the relation between the convective mass transfer and the diffusive mass transfer. Gases possess a Schmidt number of around unity, as such the smallest diffusive and smallest convective length scales are of similar size. Liquids have much higher Schmidt numbers (usually around 1000), thus the smallest length scales of diffusion are much smaller than the smallest length scales of convection. This poses an additional challenge for DNS as shown in 2.5.1.

2.4 Turbulent Reaction

To enable two fluids to react, the reactants need to be brought into direct molecular or atomic contact. Thus, in order to assess the reaction process, understanding the mixing process is crucial.

2.4.1 Turbulent Damköhler Number

The turbulent Damköhler Number represents the ratio between the turbulent time scale t_t and the chemical time scale t_c of a system

$$Da_t = \frac{t_t}{t_c}. \tag{2.59}$$

Two main regimes exist. For $Da_t < 1$, called a slow reaction, turbulent mixing happens faster than the reaction takes place. The kinetics of the reaction are paramount to the evolution of reaction over time. However, for $Da_t > 1$, the reaction is faster than the mixing. In this case, the mixing process itself is paramount to the reaction, as the chemical reaction "waits" for the turbulent mixing to supply reactants. In this case, a commonly-used simplification is *mixed is reacted*.

2.4.2 Reaction Rates

The transport equation for a species is given in equation (2.15). There the source term S_ϕ is the *chemical source term* which needs closure. In order to close this equation, this term needs to be modeled using other parameters of the flow. Also the source term for one species depends, of course, on the concentration of the other species. The Arrhenius formulation of the reaction ratei, which will be used in this work, is

$$\dot{\bar{\omega}} = kA^\alpha B^\beta e^{\frac{E_A}{RT}}. \tag{2.60}$$

2.5 Computation of turbulent flows

Analytical solutions for the Navier-Stokes equations are only known for a few, simple problems [Fri02]. While these solutions can often serve as a validation for CFD solvers, in the vast majority of cases a numerical solution needs to be applied. Three main approaches exist.

Direct Numerical Simulation or *DNS* of a flow attempts to resolve the entire spectrum of length scale that a flow possesses. Those start at the geometric dimensions of the flow at hand and end at the Kolmogorov length scales and time scales as shown in 2.2.2. This is, naturally, the most expensive approach from a computational point of view, but does not require any modeling of phenomena which happen at scales smaller than the grid resolution. On the other end of the cost-scale is the *Reynolds Averaged Navier-Stokes* or *RANS* approach. Here, only the average flow is computed directly, while all the fluctuations caused by the turbulent nature of the stream is modeled. This approach requires much lower length and time resolutions as the DNS approach, but places a heavy burden on the models for the turbulence. The *Large Eddy Simulation* or *LES* approach places itself between DNS and RANS. Large scales, which are geometry dependent and carry the majority of turbulent energy are directly computed as in DNS. In order to lower the computational effort compared to DNS, a coarser grid is chosen, and models are used to simulate the turbulence on a sub-grid scale.

2.5.1 DNS

The first part of this section will derive the requirements for the non-reacting DNS with Schmidt numbers around unity, while the second part displays the additional challenges posed by high-Schmidt number flows.

2.5.1.1 DNS with Schmidt Number Around Unity

The goal of the DNS is to directly solve the Navier-Stokes equations for all length scales so that no models are required to obtain a solution. The computational mesh needs to be fine enough that the Kolmogorov length scale η can be resolved. In order to derive the minimum grid resolution, an arbitrary flow variable is developed as a Fourier series

$$u(x,t) = \sum_{\kappa=0}^{\infty} u_\kappa(x,t) e^{i\kappa x}, \tag{2.61}$$

where κ is the wave number and u_k the amplitude of the flow variable corresponding to the wave number κ.

For a DNS, the smallest eddies with Kolmogorov length scale η have to be resolved. Thus the grid cutoff value of $\frac{\pi}{\Delta}$ has to be smaller than the wavenumber k_η of those eddies. Thus, according to

$$\Delta < \frac{\pi}{k_\eta}. \tag{2.62}$$

Assuming an equidistant grid, the largest length scale L will cover the number of grid points n as

$$n\Delta \geq L. \tag{2.63}$$

Thus, as shown by Poinsot and Veynante [PV05], the minimum number of grid points in this case is

$$n^3 = Re_t^{\frac{9}{4}}. \tag{2.64}$$

with the *turbulent Reynolds number* being defined as

$$Re_t = \frac{k^2}{\varepsilon\nu}. \tag{2.65}$$

Equation (2.64) thus places a practical limit on the problems which can be solved by DNS. Today, the largest DNS performed are usually between ten and about a hundred billion grid points. The computational requirements of a DNS are further increased by the fact that the DNS is always a transient simulation, so that the time step size that fulfills at least the CFL (Courant-Friedrich-Levy) condition must be chosen, thus

$$\Delta t < CFL\frac{\Delta}{U}, \tag{2.66}$$

with U as a typical flow velocity that is rarely exceeded. Thus, if the velocity is increased, smaller time steps need to be used as well as a finer grid (due to the increased Reynolds number).

2.5.1.2 Higher Schmidt Numbers in DNS

The problem of the very large number of grid points is further increased by the Schmidt number as seen in 2.3 in case of mixing. While in gaseous flow the resolution requirements are largely the same as for the pure flow field, liquids have a high Schmidt number and thus require a much finer spatial resolution for the

diffusive length scales, otherwise the too coarse grid imposes artificial diffusivity. Roughly assuming a Schmidt number of 1000 for a liquid, equation (2.58) thus demands a grid that has about 30000 times as many grid points to resolve the mixing length scales compared to a grid that only resolves the turbulent length scales. In order to minimize computational requirements, DNS can greatly benefit from advanced meshing techniques like adaptive meshes or multi grid methods, where the fine resolution is present only where the turbulence demands it. Those techniques can reduce the number of required grid points by orders of magnitude.

A solution for high Schmidt number was suggested by Schwertfirm and Manhart[SM07, BMPW10]. It decouples the solution of the velocity field from the solution of the scalar field. For each time step, the velocity is computed first on a grid which fulfills the requirements of the DNS. After that, the scalar field can either be computed by a DNS on a finer grid to which the velocity fields are interpolated, or the same grid as for the velocity field can be used and a LES for the scalar field is done thereon, in a *Semi-DNS* approach.

2.5.2 RANS

In RANS, the Navier-Stokes equations are averaged, i.e. each flow variable is decomposed into a mean value and a fluctuation, such as:

$$\Psi = \overline{\Psi} + \Psi'' . \tag{2.67}$$

where $\overline{\Psi}$ is the mean part and Ψ'' is the fluctuation. It is required that the mean of the fluctuation needs to be zero, $\overline{\Psi}'' = 0$. This simple decomposition is called the *Reynolds Averaging*. Another typical decomposition is the mass averaged decomposition or *Favre Averaging* of flow values as

$$\Psi = \widetilde{\Psi} + \Psi' , \tag{2.68}$$

$$\widetilde{\Psi} = \frac{\overline{\rho\Psi}}{\overline{\rho}} . \tag{2.69}$$

Here, also, the restriction $\overline{\Psi}' = 0$ applies. Using equation (2.68) and equation (2.69) on equation (2.5) and equation (2.8) yields then the transport equations used for a RANS model

$$\frac{\partial \overline{\rho}}{\partial t} + \frac{\partial \overline{\rho}\widetilde{u}_i}{\partial x_i} = 0, \tag{2.70}$$

$$\frac{\partial \overline{\rho}\widetilde{u}_i}{\partial t} + \frac{\partial \overline{\rho}\widetilde{u}_i\widetilde{u}_i}{\partial x_j} = -\frac{\widetilde{p}}{x_i} + \frac{\partial \widetilde{\tau}_{ij}}{\partial x_j} - \frac{\widetilde{\overline{\rho}u_i'u_j'}}{x_j} . \tag{2.71}$$

As can be seen, these equations contain the unclosed term $\widetilde{u_i'u_j'}$, the so called *Reynolds Stress Tensor* which needs to be modeled.

2.5.2.1 Turbulent Viscosity

Boussinesq assumed that the momentum transfer performed by the eddies can be modeled with the *eddy viscosity*, much like the molecular viscosity performs molecular momentum transfer. Boussinesq also assumed that the Reynolds stresses τ_{ij} are proportional to the traceless mean strain rate tensor,

$$\tau_{ij} = 2\mu_t S_{ij}^* - \frac{2}{3}\rho k \delta_{ij}, \tag{2.72}$$

with k as the turbulent kinetic energy as described in equation (2.35) The traceless strain tensor is computed from the strain tensor as

$$S_{ij}^* = S_{ij} - \frac{1}{3}\frac{\partial u_k}{\partial x_k}\delta_{ij}. \tag{2.73}$$

The two tensors are identical for incompressible flows as in this case $\frac{\partial u_k}{\partial x_k} = 0$, or

$$-\widetilde{u_i'u_j'} = 2\nu_t \widetilde{S_{ij}} - \frac{2}{3}k\delta_{ij}. \tag{2.74}$$

2.5.2.2 Turbulence Models for RANS

Primary task of RANS modeling is the computation of the turbulent viscosity ν_y introduced in equation (2.74), or introducing a set of transport equations for the Reynolds Stresses themselves. Thus, RANS models can be divided into different complexities.

- Zero-equation models, which do not use separate transport equations to obtain the turbulent viscosity. A local equilibrium for the turbulence is assumed, which has been shown to be questionable [Piq02].
- Single equation models, which only posses a transport equation for the turbulent kinetic energy.
- Two equation models, like the highly popular and successful k-ε and k-ω models, which have one additional transport equation for either the turbulent dissipation (ε) or frequency (ω).

- Higher models which have a larger number of transport equations like the Reynold Stress Model, where separate transport equations are solved for the Reynolds stresses $\widetilde{u_i' u_j'}$.

Approaches exist where several different turbulence models are used for different regions of the computational domain. As such, the various strengths of the different models can be exploited.

2.5.3 LES

The first part of this section shows the spatial filtering of the Navier-Stokes equation in order to obtain the LES equation, along with the unclosed terms that originate therein. In the second part the most popular models for the closure of these terms are given.

2.5.3.1 Filtering of the Navier-Stokes Equations

In LES, the *averaging* approach in RANS is replaced by a *filtering* approach in LES, where only large eddies are completely resolved by the grid. In a wavenumber space, this filter is a low-pass filter which cuts off the high-wavenumber parts, i.e. the small eddies. As in RANS, the effect of those eddies onto the flow has to be modeled. The filtering also produces another fundamental difference between RANS and LES. While RANS, due to its averaging nature usually produces a stationary result (although unsteady RANS or URANS methods have been suggested), LES is inherently a transient method. However, it is generally assumed that the smaller scales are more homogeneous and isotropic in nature than the larger turbulent scales. As such, LES turbulence models are simpler than their RANS counterparts. A few common LES models are shown below. In order to do LES, the equations that need to be solved on the coarser grid need to be spatially filtered, and unclosed terms need to be either modeled or neglected.

A flow value ϕ in LES is separated into two fractions, the resolved scales $\overline{\phi}$ and the sub-grid scales ϕ', so that

$$\phi(x_i,t) = \overline{\phi}(x_i,t) + \phi'(x_i,t), \tag{2.75}$$

where the resolved parts are the results of a low-pass filtering and the sub-grid scales are the results of the high-pass filtering. From a physical point of view, it is easiest to work with a *spectral representation* of the filter. However, the Fourier

transformation is rarely known for actual CFD simulations outside of homogeneous isotropic turbulence. Three commonly used filters are:

- The sharp Fourier cutoff filter

$$F(x_i) = \frac{2}{\Delta_i} \frac{\sin(2\pi \frac{x_i}{\Delta_i})}{2\pi \frac{x_i}{\Delta_i}}. \tag{2.76}$$

  This is called a sharp cutoff filter due to the fact that all wavelengths below the cutoff wavelength are untouched, while wavelengths above the cutoff are completely eliminated, thus, equation (2.76) becomes in spectral space

$$\hat{F}(k_i) = \begin{cases} 1, & \text{if} |k_i| \leq k_{cutoff} \\ 0, & \text{otherwise} \end{cases} \tag{2.77}$$

  with $\hat{F}$ as the filter operation in Fourier space.

- The Gaussian filter

$$F(x_i) = \left(\frac{6}{\pi \Delta_i^2} \right) e^{\left(-\frac{6x_i^2}{\Delta_i^2} \right)}. \tag{2.78}$$

  is the physical space representation of a Gauss function in spectral space

$$\hat{F}(k_i) = e^{\left(-\frac{\Delta_i^2 k_i^2}{24} \right)}. \tag{2.79}$$

- The top-hat filter, also called the box filter, is the standard intrinsic filter of LES solvers that do not compute in spectral space. In this case, the kernel is defined as

$$F(x) = \begin{cases} \frac{1}{\Delta_i}, & \text{if } x_i \leq \frac{\Delta_i}{2} \\ 0, & \text{otherwise} \end{cases} \tag{2.80}$$

  The spectral representation of this filter is

$$\hat{F}(k_i) = \frac{\sin\left(\frac{1}{2} k_i \Delta_i\right)}{\frac{1}{2} k_i \Delta_i}. \tag{2.81}$$

  The drawback of this filter can be seen in equation (2.81): This filter influences all wave numbers, even very low ones (i.e. well resolved scales). This influence grows the closer the wave number is to the cutoff wavelength.

A projector is an idempotent filter which fulfills the requirement $FF = F$.

As shown by Kim [Kim04], the discretization of the computational domain serves as an implicit filter in CFD simulations. However, this implies that wave numbers that are higher than the intrinsic cutoff wave number of the computational grid are neglected. As these wave numbers still have an effect on lower (i.e. resolved) wave numbers due to the nonlinear nature of the momentum equation, this effect needs to be modeled.

Applying the filtering function to equation (2.8), assuming that filtering and differentiation are commutative [GM95]

$$\overline{\frac{\partial \phi}{\partial t}} = \frac{\partial \overline{\phi}}{\partial t}, \tag{2.82}$$

$$\overline{\frac{\partial \phi}{\partial x_i}} = \frac{\partial \overline{\phi}}{\partial x_i}, \tag{2.83}$$

yields the filtered momentum equation, for incompressible flows

$$\frac{\partial \overline{u}_i}{\partial t} + \frac{\partial}{\partial x_j}\overline{u}_i\overline{u}_j = \nu \frac{\partial}{\partial x_i}\frac{\partial \overline{u}_i}{\partial x_i} - \frac{\partial \overline{p}}{\partial x_i} - \frac{1}{\rho}\frac{\partial \tau_{ij}}{\partial x_j}. \tag{2.84}$$

The unclosed term

$$\tau_{ij} = \overline{u_i u_j} - \overline{u}_i\overline{u}_j \tag{2.85}$$

in equation (2.84) are the sub-grid stresses. This term is the primary target for modeling efforts of single-phase LES.

It has been suggested by Leonard [Leo74] to decompose equation (2.85) as

$$\tau_{ij} = L_{ij} + C_{ij} + R_{ij}. \tag{2.86}$$

Equation (2.86) splits the sub-grid scale stress tensor into three parts:

- The Leonard-Stresses, which can be computed from resolved values as

  $$L_{ij} = \overline{\overline{u}_i\overline{u}_j} - \overline{u}_i\overline{u}_j. \tag{2.87}$$

  Using an ideal filter as presented above will cause the Leonard Stresses to vanish. In most of the current CFD codes, these stresses are assumed to be zero even though a non-ideal filter is employed.

- The Cross-Stresses which show the interaction between the resolved and the sub-grid scales

  $$C_{ij} = \overline{\overline{u}_i u'_j + u'_i\overline{u}_j}. \tag{2.88}$$

- The Reynolds-Stresses is then the remainder of the stress tensor

$$R_{ij} = \overline{u_i' u_j'}. \tag{2.89}$$

This part is the actual influence of the sub-grid scale fluctuations on the filtered flow.

2.5.3.2 LES Models

The most popular models for LES are the Smagorinsky model, along with its dynamic extension, and the turbulent kinetic energy model. Next to those models, a variety of other models of different complexity exist.

Smagorinsky Model Smagorinsky [Sma63] developed the first LES model in 1963. For simplicity's sake, this model does not introduce additional transport equations to the solution, but simply adds an algebraic closure for the sub-grid scale turbulent viscosity ν_t

$$\nu_t = (C_S \Delta)^2 \overline{S}_{ij}, \tag{2.90}$$

$$S_{ij} = \left(2\overline{D}_{ij} D_{ij}\right)^{0.5}. \tag{2.91}$$

Here C_S is a constant that has to be selected prior to the computation, which is usually in the range of 0.1 to 0.2. Δ is the width of the filter; for non-cubic grids, $\Delta^3 = V$ with V as the volume of the cell.

Note that the original model assumes that in equation (2.86) $L_{ij} + C_{ij} = 0$ and the model applies to R_{ij} only. However, since L_{ij} can be directly computed from the filtered velocity field, other applications of the Smagorinsky model have applied it to $C_{ij} + R_{ij}$.

Dynamic Smagorinsky Model The previous model has the drawback of selecting a single value for C_S for the entire domain and every time step. This usually leads to a gross overestimation of the dissipation near walls. Germano and Lilly [GPMC91, Lil92] have suggested to compute a value for C_S for each cell dynamically. This is achieved by using a coarser test filter (denoted by $\widehat{\ }$) on the resolved scales, compute the turbulent viscosity from there and derive C_S from this viscosity.

The Germano identity

$$L_{ij} = T_{ij} - \widehat{\tau}_{ij} \tag{2.92}$$

is the difference between the residual stress tensor of the test filter T_{ij} and the residual test tensor of the grid $\widehat{\tau}_{ij}$, which are computed as

$$T_{ij} = \widehat{\overline{u_i u_j}} - \widehat{\overline{u}}_i \widehat{\overline{u}}_j, \tag{2.93}$$

$$\widehat{\tau}_{ij} = \widehat{\overline{u}_i \overline{u}_j} - \widehat{\overline{u}}_i \widehat{\overline{u}}_j. \tag{2.94}$$

The model then yields for the model constant

$$C_S = \sqrt{\frac{L_{ij} M_{ij}}{M_{ij} M_{ij}}}, \tag{2.95}$$

with

$$M_{ij} = 2\overline{\Delta}^2 \left(\overline{\left|\widehat{S}\right| \widehat{S}_{ij}} - \left(\frac{\widehat{\Delta}}{\overline{\Delta}} \right)^2 \left|\overline{\widehat{S}}\right| \overline{\widehat{S}_{ij}} \right), \tag{2.96}$$

where $\widehat{\Delta}$ and $\overline{\Delta}$ represent the filter width on the test filter and the grid filter respectively.

Turbulent Kinetic Energy Model Various other LES Models have been developed since the Smagorinsky Model shows a number of drawbacks. One of the most obvious ones is that it does not take the history of a fluid particle into account. In order to make this possible, Kim [Kim04] has developed a model where the sub-grid turbulent viscosity is proportional to the square root of the sub-grid turbulent kinetic energy k, for which a transport equation is formulated which is

$$\frac{\partial k}{\partial t} + \frac{\partial \overline{u}_j}{\partial k} = -\tau_{ij} \frac{\partial \overline{u}_i}{\partial x_j} - C_\varepsilon \frac{k^{\frac{3}{2}}}{\Delta} + \frac{\partial}{\partial x_j} \left((\nu + \nu_t) \frac{\partial k}{\partial x_j} \right). \tag{2.97}$$

Then the sub-grid turbulent viscosity can be computed as

$$\nu_t = \sqrt{k} C_k \Delta. \tag{2.98}$$

In order to maximize the performance of this model, the model parameters are determined by the dynamic procedure similar to the dynamic Smagorinsky model in the previous paragraph.

Scalar Transport Equation and Models Comparable to the unclosed terms in the filtered momentum equation (2.84) the filtered scalar transport equation,

$$\frac{D\overline{\phi}}{Dt} = \frac{\nu}{Sc}\frac{\partial^2\overline{\phi}}{\partial x_i^2} - \frac{\partial \tau_{i\phi}}{\partial x_i} + \overline{\dot{\omega}}, \tag{2.99}$$

contains on the one hand the unclosed term $\tau_{i\phi}$, the *sub-grid scale scalar flux*, which is defined as

$$\tau_{i\phi} = \overline{u_i\phi} - \overline{u}_i\overline{\phi}. \tag{2.100}$$

In analogy to the eddy viscosity models, which are used to close the sub-grid scale turbulence, the sub-grid scale mixing can be modeled by eddy diffusivity models, where the turbulence accelerates the mixing. This has been suggested by Eidson [Eid85], so that the transport equation can be closed as

$$\tau_{i\phi} = -\Gamma_{SGS}\frac{\partial\overline{\phi}}{\partial x_i}, \tag{2.101}$$

where Γ_{SGS} is the eddy diffusivity that is obtained similar to the Smagorinsky model as

$$\Gamma_{SGS} = 2\frac{(C_S\Delta)^2}{Sc_{SGS}}|\overline{S}_{ij}|. \tag{2.102}$$

Here, Sc_{SGS} is the sub-grid scale Schmidt number, which usually takes a value of approximately 0.4 [PS00]. The model constants in this equation can be determined dynamically in analogy to the procedure shown in the previous section for the eddy viscosity models. It should be noted that for high Schmidt number flows the sub-grid scale eddy diffusivity far outweighs the molecular diffusivity, which can then be neglected completely.

Closure of the second unclosed term in equation (2.99), $\overline{\dot{\omega}}$, called the *filtered reaction rate* is one of the central topics of this work; the fundamental approach is shown in the next chapter.

3 Mixing Models

This chapter will explain the use of mixing models in the present work. Section 3.1 will give an overview of mixing models, their properties and some commonly used models, while the subsequent sections will explain the adaptation of the Modified Curl model, which has proven to be the most applicable and most robust solution to the problem at hand.

3.1 Fundamentals of Mixing Models

As seen in chapter 2, an LES or RANS simulation, as opposed to DNS, contains a certain amount of unresolved unmixedness within a computational cell. Chapter 4 will show that PDF methods are effective in modeling this unmixedness. It was also explained how transported PDF and jPDD methods require mixing models to represent the particle interaction in order to actually model the mixing of the fluid on a molecular scale. These mixing models, called *particle-interaction models*, work by moving particles in the composition space from their initial position towards the mean value. Thus, a mixing model will evolve any initial distribution to single Dirac peak after a sufficiently large number of *mixing events*, i.e. a single particle interaction process.

Based on the description of molecular mixing by Pope [Pop94], a number of requirements that a mixing model shall posses in order to correctly model a physical molecular mixing process, were derived. The full set of requirements can be found in Meyer and Jenny [MJ06].

1. the mean of the scalars must remain unchanged
2. the variance of the scalars must decrease
3. in homogeneous turbulence, the joint PDF of inert scalars should relax to a joint Gaussian
4. realizability has to be honored, i.e. scalars have to remain within the allowable region

5. insensitivity with respect to linear transformations in scalar space and independence of passive scalars
6. localness in scalar space
7. velocity and scalar gradients must remain uncorrelated
8. correct dependence on scalar length scales
9. correct dependence on Reynolds, Schmidt and Damköhler numbers

3.2 Mechanical-to-Scalar Time Scale Ratio

For transported PDF methods, most of the mixing models require a modeling parameter which is the mixing time scale. As seen in a review done by Pope [Pop85], the suggestion of having a fixed mechanical-to-scalar time scale ratio of 2.0 still is the most widely used, thus

$$\tau_\phi = 2\frac{\tau}{C_\phi}, \tag{3.1}$$

with τ_ϕ as the scalar time scale, τ as the turbulent time scale and C_ϕ as the model constant for the time scale ratio. As explained earlier, molecular diffusion can be neglected with respect to turbulent diffusion at sufficiently high Reynolds numbers. Fox [Fox03] also shows that at high Schmidt numbers, the mechanical-to-scalar time scale ratio is constant. Eswaran and Pope [EP88] have performed DNS simulations which show that independent of the initial distribution of the scalar length scales, the system tends towards a final mechanical-to-scalar time scale ratio of 2.0. However, in both instances this constant ratio is only valid for fully developed spectra. As will be shown later in chapter 5, this assumption is not necessarily true for the entire domain.

Methods that assume not fully developed spectra and thus a non universal mechanical-to-scalar time scale ratio for the entire domain have been developed in the past, for example by Fox [Fox03]. Also, chemical reactions influence the time scale ratio [Pop85]. As a result, methods which take this effect into account have been suggested [CWP07].

3.3 Mixing Models

This chapter will present a number of existing mixing models along with their properties. This will cover only a small number of mixing models available today.

Due to the complex nature of the mixing process and the vastly different numerical approaches, for example RANS versus LES, no universal mixing model has yet been developed.

3.3.1 IEM / LMSE

The Interaction By Exchange With The Mean, short IEM Model, was suggested by Villermaux and Devillon in 1972 [VD72]. A physically different approaching that led to the same model was chosen by Dopazo and O'Brian called LMSE Model [DO74]. Here the change of composition of a particle is described as

$$\frac{df^{(i)}}{dt} = -\frac{1}{2} C_f \langle \omega \rangle \left(f^{(i)} - \langle f \rangle \right), \tag{3.2}$$

with $\langle \omega \rangle$ as the mean turbulence frequency and C_f as the mechanical-to-scalar time scale ratio. This ratio is assumed to be around 2 for high Reynolds number flows as shown in [Fox03] for fully developed spectra.

In homogeneous turbulence, all particles relax towards the mean of the ensemble with a rate that is proportional to its distance from the mean. This distance is measured in state space, not physical space. Thus, this model is shape preserving and will not relax to a Gaussian as required (see 3.1)

From (3.2) the decay of scalar variance $\left\langle f'^2 \right\rangle$ can be derived as

$$\frac{d}{dt} \ln \left\langle f'^2 \right\rangle = -C_f \langle \omega \rangle . \tag{3.3}$$

3.3.2 Modified Curl

The Modified Curl model by Janicka, Kolbe and Kollmann in 1977 [JJ79] is based on the standard model by Curl [Cur63]. Here, as opposed to the previous model, two particles are randomly chosen from the ensemble and their compositions are altered so that they both translate towards the mean value. As this model is the foundation for the new model developed in this thesis, it is explained in detail in section 3.4.

3.3.3 Mapping Closure

A different mixing model, which starts from a Gaussian reference field, has been suggested by Pope [Pop91] in 1991. It implies localness in scalar space by using the condition

$$f^i \leq f^{i+1}. \tag{3.4}$$

The distribution with a total number of N particles then develops as

$$\frac{df^{(1)}}{dt} = \frac{1}{2}C_f' \langle\omega\rangle \left[B_{1+\frac{1}{2}}\left(f^{(2)} - f^{(1)}\right)\right], \tag{3.5}$$

$$\frac{df^{(i)}}{dt} = \frac{1}{2}C_f' \langle\omega\rangle \left[B_{i+\frac{1}{2}}\left(f^{(i+1)} - f^{(i)}\right) + B_{i-\frac{1}{2}}\left(f^{(i-1)} - f^{(i)}\right)\right], \tag{3.6}$$

$$\text{for } i = 2 \ldots n_p - 1$$

$$\frac{df^{(n_p)}}{dt} = \frac{1}{2}C_f' \langle\omega\rangle \left[-B_{n_p-\frac{1}{2}}\left(f^{(n_p)} - f^{(n_p-1)}\right)\right]. \tag{3.7}$$

3.3.4 Euclidian Minimum Spanning Tree

Subramaniam and Pope [SP98] introduced a significantly more complex mixing model, the Euclidian Minimum Spanning Tree, EMST model. One of the main goals of this model was to preserve the localness of the distribution. If, for each time step, the whole distribution is taken to construct the spanning tree, the distribution has the tendency of stranding, i.e. the formation of distinct branches, which is unphysical. In order to prevent this, the EMST model randomly selects a subset of the distribution, which then interacts. By actively controlling the mixing parameter, the EMST can be adjusted to perform an exponential variance decay, as demanded by high Reynold number flows.

3.3.5 PSP

Mayer and Jenny [MJ04, MJ06] have suggested a mixing model based on *parametrized scalar profiles*, which is an extension of the IEM model discussed previously. The scalar field is assumed to be describable by scalar profiles, which are sinusoidal in nature. The profiles are parametrized by four values, f_- and f_+,

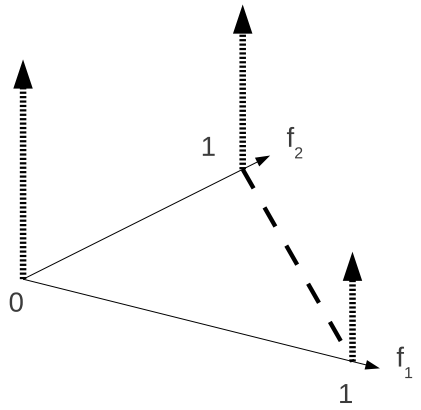

Figure 3.1: Initial distribution for the mixing model. Dashed line indicates the boundary of the physically accessible state-space: The sum of mixture fractions can never exceed unity

which are the minimum and maximum value of the profile, λ which is the width of the profile and τ_f as the relaxation time. The profile then evolves as

$$f(x,t) = e^{\frac{-t}{\tau_f}} \frac{f_+ - f_-}{2} \sin\left(\frac{x\pi}{\lambda}\right) + f_c, \tag{3.8}$$

where x is the coordinate local to the profile and $f_c = \frac{f_+ + f_-}{2}$ is the center value of the profile. This model requires additional models or transport equations for the model parameters. It however shows very promising results [MJ06].

3.4 A Biased, Multi-Variate Mixing Model

The mixing models shown in the previous section have been used in transported PDF methods, where the particles that interact are indeed convected through the domain by the velocity field. This work, on the other hand, uses mixing models in a different fashion. Like in presumed PDF methods, no particles are convected by the CFD solver. Instead, transport equations for the mathematical moments of the distributions are solved. The mixing model then needs to generate a distribution

with the required set of moments. A reaction rate is then computed from this distribution.

Thus, the mixing model operates in a completely different environment than it would in transported PDF methods. There, an input distribution is given by the solver and the particle movement. The mixing model then creates a new distribution. Mixing parameters, that appear in a large number of mixing models, are determined from flow data. As such, the mixing model has a set of inputs, and properties of the *output distributions* are the result of the computation that the mixing model performs.

In this work, the only information supplied to the mixing model are the first and second order moments, called the *target values* of the output distribution. The mixing model then has to select a suitable set of input parameters from which to obtain the output distribution. The set of input parameters consists of the initial distribution and the first and second order moments of the output distribution. The mixing model needs to cope with multiple mixture fractions, i.e a *multi variate mixing model* is needed and the second order moments consist not only of the variance but of the covariance as well.

The first two requirements for mixing models shown in 3.1 are the preservation of the mean and the reduction of variance. Therefore, the mixing model is supplied with an initial distribution that already possesses the required means, and contains the maximum possible variance. This is achieved by moving all particles to the extremes of the state space. In a two-mixture-fraction setup this means a set of three Dirac peaks at the corners of the mixture fraction triangle, as seen in figure 3.1.

As discussed, the main driver behind understanding the mixing process is the determination of the reaction rate. Once the final distribution has been obtained, a reaction rate is computed from the distribution by summing up the reaction rates of each individual particles

$$\overline{\omega} = \frac{1}{N} \sum_{i=0}^{N} \dot{\omega}(f_1^{(i)}, f_2^{(i)}), \tag{3.9}$$

, and the distribution is henceforth no longer needed. A look-up table is then used to store the relation between the statistical moments on the one hand and the resulting reaction rate on the other hand, formally

$$\overline{\omega} = F\left(\overline{f}_1, \overline{f}_2, \overline{f_1'^2}, \overline{f_2'^2}, \overline{f_1' f_2'}\right), \tag{3.10}$$

, where $F(x)$ represents the look-up in the table. See figure 1.3 for a schematic overview of the process.

The LES itself never encounters actual particle distributions. It only enters the look-up table with a set of moments and obtains the reaction rate from it. The details of the distribution that generated this reaction rate is of subordinate importance and so is the intensity of the individual *mixing event*, which is the interaction of two particles.

Each mixing event has a mixing parameter associated with it, which is usually selected in some random fashion. In this work, the mixing model is based on the Modified Curl model shown earlier, and the particle selection and interaction is unchanged. However, the mixing model needs to obtain a distribution with a set of required moments. This is achieved by modifying the upper and lower boundaries of the mixing parameter for each mixing event. This process is called *biasing* of the mixing model and its pseudo random number generator. The exact biasing process will be explained in the following two sections.

The Modified Curl model then randomly selects pairs of particles $f^{(p)}$ and $f^{(q)}$ from the distribution and their compositions are changed by a mixing event. Since in this work every particle carries multiple mixture fractions $f_i, i = 1,2$ with $f_1 + f_2 \leq 1$, these are modified as

$$f_{i,n+1}^{(p)} = f_{i,n}^{(p)} + \frac{1}{2} a \left(f_{i,n}^{(q)} - f_{i,n}^{(p)} \right), \tag{3.11}$$

$$f_{i,n+1}^{(q)} = f_{i,n}^{(q)} + \frac{1}{2} a \left(f_{i,n}^{(p)} - f_{i,n}^{(q)} \right), \tag{3.12}$$

where (p) and (q) denote the two chosen particles, n and $n+1$ denote the state of the particle before and after the process and a is a randomly chosen number (called the mixing parameter), which is distributed uniformly between zero and unity.

3.4.1 Variance Adjustment

The variance V of a random variable X with the expected value $\mu = E(X)$ can be written as

$$V(X) = E\left[(X - \mu)^2 \right]. \tag{3.13}$$

In analogy to Subramaniam and Pope [SP98] it is assumed that the scalar variance decays as

$$V(n) = V_0 e^{-Cn}, \tag{3.14}$$

where V_0 represents the initial variance of the distribution, C denotes a constant that depends on the mixing parameter in equation 3.11 and n is the number of mixing processes. For uniformly distributed parameters

$$C \propto a, \tag{3.15}$$

if the number of mixing event is statistically significant.

If the mixing parameter a in equations (3.11) and (3.12) is distributed in the same fashion for each mixture fraction i, it is obviously not possible to obtain distributions that have greatly differing variances for both mixture fractions, unless the initial distribution already possesses such variances. Thus, assigning different mixing parameters a_i to each of the mixture fractions is required. The mixture fraction of the particle then is modified as

$$f_{1,n+1}^{(p)} = f_{1,n}^{(p)} + \frac{1}{2} a_1 \left(f_{1,n}^{(q)} - f_{1,n}^{(p)} \right), \tag{3.16}$$

$$f_{1,n+1}^{(q)} = f_{1,n}^{(q)} + \frac{1}{2} a_1 \left(f_{1,n}^{(p)} - f_{1,n}^{(q)} \right), \tag{3.17}$$

$$f_{2,n+1}^{(p)} = f_{2,n}^{(p)} + \frac{1}{2} a_2 \left(f_{2,n}^{(q)} - f_{2,n}^{(p)} \right), \tag{3.18}$$

$$f_{2,n+1}^{(q)} = f_{2,n}^{(q)} + \frac{1}{2} a_2 \left(f_{2,n}^{(p)} - f_{2,n}^{(q)} \right). \tag{3.19}$$

Here, a_1 and a_2 are the two different mixing parameters for the two different mixture fractions.

If different mixing parameters a_i are chosen, the decay law (3.14) for the two mixture fractions can be written as

$$V_{1;target} = V_{1;initial} e^{-C_1 n}, \tag{3.20}$$

$$V_{2;target} = V_{2;initial} e^{-C_2 n}. \tag{3.21}$$

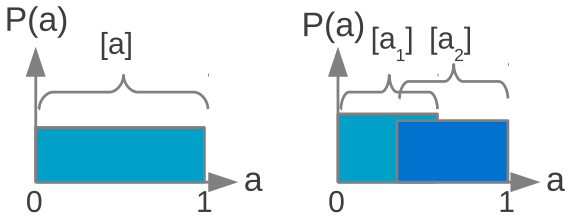

Figure 3.2: Distribution of mixing parameter for a single mixture fraction (left) and multiple mixture fractions (right). The area of both rectangles in the right case is identical.

It can be seen that if the initial and target variances are known, the number of mixing processes is canceling out and the only remaining unknown from equations (3.20) and (3.21) is the quotient of the decay velocities C_1/C_2

$$\frac{a_1}{a_2} \propto \frac{C_1}{C_2} = \frac{\ln \frac{V_{1;initial}}{V_{1;target}}}{\ln \frac{V_{2;initial}}{V_{2;target}}}. \tag{3.22}$$

It should be noted for stability reasons that a_i cannot exceed unity, which imposes a minimal number of steps required to reach the given target values for the variances. A representation of the mixing parameter distribution for two different mixture fractions can been in figure 3.2.

Thus, when two particles are selected for mixing, one (random) mixing parameter a_i is generated for *each* of the mixture fractions i. However, while the standard model has a uniformly distributed mixing parameter between 0 and 1, for multiple mixture fractions the range of the mixing parameters is reduced. This process is called the *biasing* of the random number generator. A typical variance evolution over the mixing processes is shown in Figure 3.3. It can be seen that while both mixture fractions commence at similar variances, the desired terminal variances have been reached after the same number of mixing processes. The slight deviations from the perfect e^{-x} law by both variances can be explained by the statistical nature of the selection of the mixing parameter and particles.

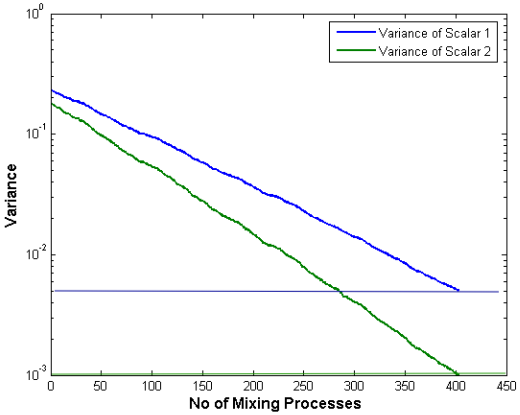

Figure 3.3: Variance decay over mixing processes for the Modified Curl Model over a total of 400 mixing processes with 1600 particles. Both target variances are met after the same number of mixing events. The target variances for each mixing parameter is indicated by the horizontal line of the same color.

3.4.2 Covariance

Distributions can have different covariances or correlations, with the covariance C of two random variables X and Y defined as

$$C(X,Y) = E\left[(X-\mu)(Y-\nu)\right], \tag{3.23}$$

with $\mu = E(X)$ and $\nu = E(Y)$ being the expected values of X and Y. The correlation $\rho_{X,Y}$ of X and Y can be interpreted as the normalized covariance (i.e. the correlation is always between -1 and 1)

$$\rho_{X,Y} = \frac{C(X,Y)}{\sqrt{V(X)V(Y)}}. \tag{3.24}$$

As opposed to distributions with a low absolute value of the correlation, which are more or less circular (as can be seen in figure 3.5a), the ones with higher correlations (absolute value) have a more elliptic shape (figure 3.5b). The slope of the semi–major axis of the ellipsis, with respect to the f_1, f_2–coordinate system, corresponds to the correlation of the distribution. This fact is exploited in the further *biasing* of the mixing process, with the objective of generating jPDDs with certain values of covariance. As seen from figure 3.4, neglecting the covariance can result in significant errors in the reaction rate. In the displayed case, there are three streams, one containing the fuel (methane), and two containing the oxidizer at different temperatures. Initially, at mixing step 0, there is no reaction as the reactants are not yet mixed at all. Then, while the variance decays, the normalized reaction rate evolves very differently between the distributions until, after a large number of mixing steps, the variances have decayed sufficiently so that the covariance is no longer a factor.

In order to obtain a distribution with a certain correlation, the mechanism used to bias the mixing parameter a_i in equations (3.11) and (3.12) is also employed for the correlation: As seen earlier, correlated functions are of elliptic nature, the correlation itself can be interpreted as the slope of the semi-major axis of the ellipse (the *correlation slope*)[1]. Hence, if the line that connects two mixing particles is parallel to the correlation slope, the mixing parameter will be selected so that these particles will mix slowly, while those particles whose connecting line is perpendicular to the correlation slope will mix more rapidly (cf. figure 3.6). This is another factor which is required to bias the pseudo-random number generator to obtain the mixing parameter for each mixing event. Because of the statistical

1 The correlation slope is measured as the angle between the semi-major axis and the X-axis.

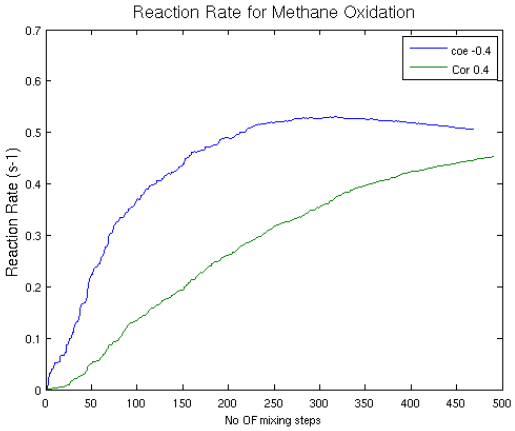

Figure 3.4: Example reaction rate of the first oxidization step of methane. Three streams are involved, one contains methane at 300K, the other two air at 600K and 1200K.

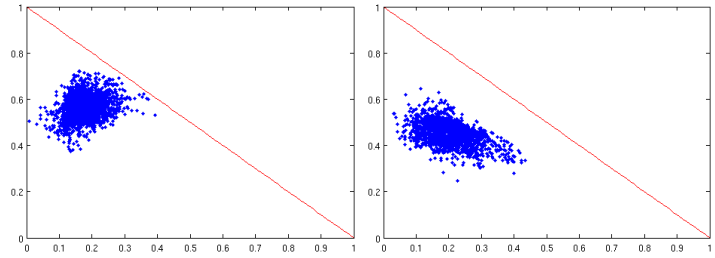

(a) Means: 0.19, 0.56
Variances: 0.002 and 0.003
Correlation: 0.24

(b) Means 0.19, 0.44
Variances: 0.004 and 0.003
Correlation: -0.48

Figure 3.5: Distributions with different correlations taken from DNS. (a) Distribution with a low (absolute value) correlation, which is more circular in nature. (b) Distribution with a higher absolute value for the correlation, it is more elliptic.

nature of the mixing process, the development of the covariance is also statistical. Due to this and the fact that the initial distribution already has a significant correlation, it is insufficient to simply adjust the mixing process along the correlation slope. In that case, the target value of the correlation would not be obtained after the same number of mixing events that are needed to obtain the target values of the variances. Hence, the following iterative scheme is applied for the correlation to meet the target value of the correlation after the correct number of mixing events:

1. Start with a *reference slope* that is parallel to correlation slope.
2. Assess the correlation after a number of mixing events so that all particles have mixed once.
3. Modify the reference slope. If the correlation is building up too fast with respect to the required number of mixing events (see section 3.4.1), reduce the reference slope with respect to the correlation slope, if the correlation is growing too slow, increase the reference slope.

Using this scheme, it can be seen that the target correlation is obtained after the correct number of mixing events. An example for the evolution of the covariance by using this method is shown in figure 3.7. The large-scale fluctuations of the correlation are the influence of the reference slope, while the small-scale fluctuations are due to the statistical nature of the mixing. At each mixing process, the reference slope was updated to meet the required correlation.

As shown previously, the biasing of the mixing parameter for variance adjustment is performed on a global level. It is selected in the beginning, depending on the initial and target variances. This is in contrast to the biasing which adjusts the co-variance of the distribution. Here, the mixing parameter is modified for each mixing event. As such, the variances and the correlation can be adjusted independently from each other.

This scheme thus ties up the two statistically independent parameters of the mixing process i.e. the variance and the correlation. The whole exercise of mixing the particle ensembles in steps is to ensure that while the variance decays, the correlation between the particle ensemble also develops and attains a value close to the target value. The magnitude of the error i.e. the difference between the target correlation and the correlation after every time step drives the adjustment to be made in the reference slope based on which the mixing parameter is determined. The functional dependency of the mixing parameter on the reference slope is treated here with sine of angle of orientation of the mixing points. It should be noted

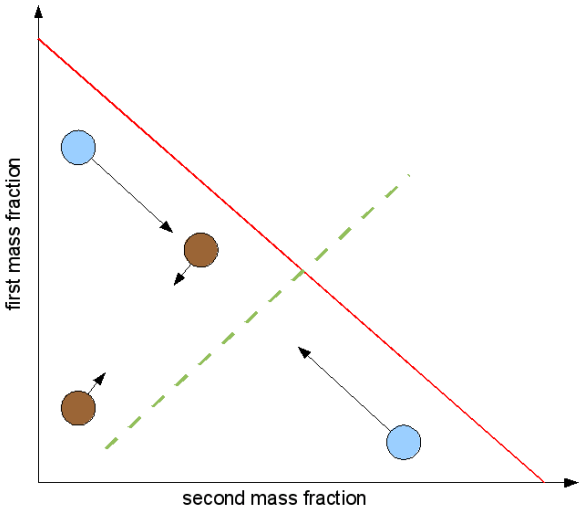

Figure 3.6: Principle of covariance based mixing: As the blue particles are perpendicular to the reference slope (dashed line), they mix more rapidly as the brown particles, which are more in-line to the reference slope (mixing intensity indicated by arrow length)

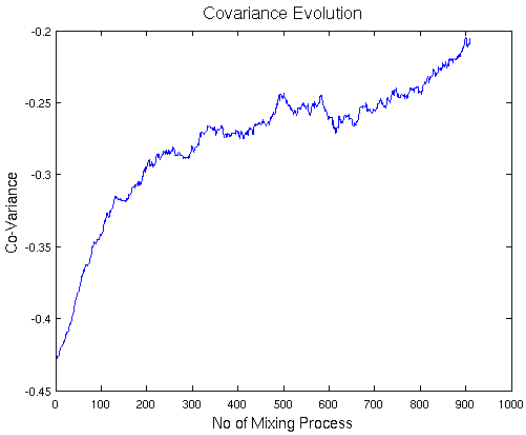

Figure 3.7: Evolution of the covariance of a given distribution. The initial covariance is determined by the initial Dirac–Delta peaks, the targeted covariance is -0.2

that the mixing parameter is only adjusted to the extent where decay of variance is nearly equal to that given by the decay law for a given time step and hence the correction in the covariance of the distribution continues till the variance decays to the required values [FMP09].

Concerning the requirements for mixing models presented in 3.1, it should be mentioned that the new mixing model, which is based on the Modified Curl model, does not fulfill any requirements that the Modified Curl itself does not fulfill. Furthermore, as the mixing model is employed in an offline step for this work, dependence on flow parameters like scalar lengths scale or Reynolds, Schmidt and Damköhler numbers is not given. The first four requirements however, are met.

4 Probability Density Functions

This chapter will give an overview of methods employing probability density functions (PDF methods) and their associated transport equations in order to close the chemical source term.

In the beginning of this chapter, section 4.1 will show how PDF methods can be used to close the chemical source term. Section 4.2 will then introduce the basic PDFs that can describe stochastic variables such as the velocity or the composition of the flow field.

The second part of this chapter will then explain various PDF approaches such as Filtered Density Functions (FDFs) for LES applications in section 4.3. The main representations of PDFs, namely presumed PDF methods and transported PDF methods will then be explained in section 4.4. The new representation, joint presumed discrete distributions (jPDD) are explained in 4.5.

The final part of this chapter shall then introduce the transport equations for PDF methods. At first, the general mechanims for deriving a transport equation of the PDF is explained in 4.6. As the present work lends transport equations for the statistical moments of a distribution, those will be introduced.

While the basic scalar transport equation has already been introduced in chapter 2, the transport equations for the variance and the covariance will be shown here in section 4.7. Additonally the section explains and derives the models required for the closure of said transport equations.

4.1 Closure for the Chemical Source Term

Equation (2.99) is the fundamental transport equation for the species concentration. Besides the sub-grid scale scalar flux, $\tau_{i\phi}$, which has been explained earlier, it contains another unclosed term which is the filtered reaction rate $\overline{\dot{\omega}}$. The simplest approach for this term is only to take the means of the mixture fractions into account and to compute the reaction rate from there, as in

$$\overline{\dot{\omega}} = f\left(\overline{f}_1, \overline{f}_2\right). \tag{4.1}$$

However, this assumes that the scalar field is perfectly mixed on a sub-grid level, i.e. the concentration is free of sub-grid scale fluctuations. It was shown [Bra05] that this assumption is usually not valid, the *sub-grid scale unmixedness* has to be taken into account. One approach to determine the filtered reaction rate is to use an *PDF* or *Probability Density Function* approach, where the reaction rate would take the variances and covariance into account. For a simple system with two concentrations, the filtered reaction rate would then be

$$\overline{\dot{\omega}} = \iint \dot{\omega}\left(f_1, f_2\right) P\left(f_1, f_2\right) df_1 df_2. \tag{4.2}$$

In this work, PDFs are usually represented by particle ensembles, in which case 4.2 results in

$$\overline{\dot{\omega}} = \frac{1}{N} \sum_{i=0}^{N} \dot{\omega}(f_1^{(i)}, f_2^{(i)}), \tag{4.3}$$

with N as the number of particles and (i) denoting the i-th particle of the distribution.

4.2 Flow Description Using PDFs

The Navier-Stokes equations described in chapter 2 can be used to exactly predict the evolution of a flow field. However, due to the non-linearity of the equations, slight variations in the initial or boundary conditions can result in large variations of the resulting flow field. However, in most cases, a single realization of the resulting flow field is only of minor interest. Instead, a statistical description of the flow can be used. As such, the flow variables can be treated as statistical variables.

4.2.1 One-Point, Velocity PDF

If a fixed point (x, t) is taken in space time, the PDF F of the velocity component u_1 is defined as [Fox03]

$$F_{u_1}(U_1;x,t) \equiv P\{U_1 \leq u_1(x,t) < U_1 + dU_1\}. \tag{4.4}$$

If a statistically significant number of flow realizations are present, (4.4) shows the probability that the variable u_1 at the position (x,t) is between U_1 and $U_1 + dU_1$ in the *sample space*.

4.2.2 One-Point Velocity Composition PDF

Turbulent mixing can be described using the one-point joint velocity/composition PDF as

$$F_{u_i,\phi}(U,\Phi;x,t) \equiv P\{[U_i \leq U(x,t) < U_i + dU_i] \cap [\Phi \leq \phi(x,t) < \Phi + d\Phi]\} \tag{4.5}$$

4.2.3 One-Point Composition PDF

By integrating (4.5) over the entire velocity sample space,

$$F_\phi(\Phi;x,t) = \iiint_{-\infty}^{+\infty} F_{u_i,\phi}(U,\Phi;x,t)dU_i \tag{4.6}$$

the one-point composition PDF is obtained, resulting in

$$F_\phi(\Phi;x,t) \equiv P\{\Phi \leq \phi(x,t) < \Phi + d\Phi\}, \tag{4.7}$$

with ϕ as the scalar in question and Φ as the point in sample space that is being sought. Removing the velocity information implies the following restrictions [Fox03]

- Due to the missing information about the velocity field, a turbulence model needs to supply mixing information by the velocity field (i.e. turbulence).
- The link between the scalar field and the velocity fluctuations, i.e. the scalar fluxes is lost. A scalar flux model is required for closure.

- The information about the scalar dissipation rate is lost. The variance decay has to be provided by another means, such as a mixing model or a direct model for the scalar dissipation rate in the transport equation for the scalar variance. Such a model is shown in section 4.6.

Describing the mixing state by using a PDF method with a one-point PDF is a common approach to simulate mixing phenomena, while models for the turbulence, scalar fluxes and scalar dissipation rates are employed.

4.2.4 One-Point Joint PDF

Also, if two mixture fractions or concentrations are present, they can be written into a single joint composition PDF

$$F_{\phi_1,\phi_2}(\Phi_1,\Phi_2;x,t) \equiv P\{[\Phi_1 \leq \phi_1(x,t) < \Phi_2] \cap [\Phi_2 \leq \phi_2(x,t) < \Phi_2]\} \tag{4.8}$$

4.3 Filtered Density Functions

Initially, PDF methods have been formulated for RANS computations, where only the mean values of the flow field are directly computed. The PDFs could then be used to model the fluctuating part of any variables. However, the PDF approach has been adopted for the use in LES context. In LES the PDF is then used to model only the sub-grid scale part, which is not directly simulated. Formally, the PDF itself is filtered leaving only the sub-grid scale *filtered density function*. The difference between a full PDF and an FDF in LES context shall be shown here. As seen in chapter 2, an ideal LES filter cuts off all wave numbers κ greater than a cut-off value κ_c. Thus, the unresolved velocity field $u_i(x_i,t)$ in spectral space is

$$u_i(x_i,t) = \sum_{|\kappa|>\kappa_c} \widehat{U}_\kappa(t) e^{i\kappa x} \tag{4.9}$$

with $\widehat{U}$ representing the velocity in Fourier space. The filtered density function suggested by Pope [Pop00] is defined as

$$h_U(V;x,t) = \int_{-\infty}^{+\infty} \delta\left[U(r,t) - V\right] G(r-x)dr. \tag{4.10}$$

This FDF is a random variable in the sense that it is different for each flow realization. This in contrast to the velocity PDF which is defined on the sub-ensemble of all realizations of the flow that possesses the same filtered velocity field [Fox03].

4.4 Different PDF Approaches

Two main approaches exist for PDF methods. On the one hand are presumed PDF methods where the shape of the distribution is predetermined by an analytical function. The number of parameters that this function possesses then equals the number of transport equations that need to be solved.

On the other hand, transported PDF methods do not predetermine the shape of the PDF. One of the most successful approaches to these methods is the *Monte-Carlo* approach. Here, the PDF is represented by a large number of particles.

This work introduces a new approach to describing the PDF which is positioned in the middle between presumed PDF and transported PDF approaches.

The three different approaches shall be explained in this section, along with a short comparison.

4.4.1 Presumed PDFs

The most straightforward approach is to presume a given functional form of the PDF [GB87, Gut91]. Most commonly used functions are for example Gaussian functions, clipped Gaussian functions and Beta functions. This approach is computationally inexpensive since it only adds transport equations for the parameters or statistical moments that the function requires. For the (clipped or unclipped) Gaussian, these would be for example the means and variance, or the first and second order moment. Due to the simplicity of the approach, it proves also to be numerically stable.

While this approach has been applied with success to a number of technical applications, the main drawback still remains: There is no physical derivation for the shape of the PDF, the underlying 'presumed' function will always be arbitrarily chosen.

For a presumed PDF, the filtered reaction rate can be derived from equation (4.2) as

$$\overline{\omega} = \iint \dot{\omega}(f_1, f_2) P\left(f_1, f_2; \overline{f}_1, \overline{f}_2, \overline{f_1'^2}, \overline{f_2'^2}, \overline{f_1' f_2'}\right), \tag{4.11}$$

with $\overline{f}$ representing the means, $\overline{f'^2}$ representing the variance and $\overline{f'_1 f'_2}$ representing the covariance. The term $\left(f_1, f_2; \overline{f}_1, \overline{f}_2, \overline{f'^2_1}, \overline{f'^2_2}, \overline{f'_1 f'_2}\right)$ is the probability that the tuple f_1, f_2 occurs if the input parameters are $\overline{f}_1, \overline{f}_2, \overline{f'^2_1}, \overline{f'^2_2}, \overline{f'_1 f'_2}$. Brandt [Bra05] shows that neglecting the covariance can result in significant errors in the reaction rate.

One of the most significant limitations of the presumed PDF approach is the low number of degrees of freedom: The function that has been selected to represent the mixing state of the cell determines the number of transport equations that are needed: Each parameter of the function requires one transport equation.

4.4.2 Transported PDFs

Transported PDFs are the other end of the computational cost scale. In this approach, a large number of (mass less) particles is introduced into the flow field. The particles themselves carry the property or multiple properties of the flow that is of interest, for example mixture fractions. The PDF is then represented by the ensemble of all particles that are present in a single computational cell at a given point in time. However, this approach is, on the one hand, computationally expensive, as it involves tracking a large number of particles through the field, since, for stable statistics, each cell needs to contain a sizable number of particles. Thus, the number of particles that need to be tracked, far exceeds the number of cells in the computational domain. Also, algorithms for particle management need to be introduced, since particles might cluster in large numbers in a single cell, while other cells might become devoid of particles over time. The particle management has to add or remove particles from those cells without altering the statistics of the ensemble in the cell.

Transported PDF methods require modeling of particle interaction. If the particles carry, for instance, information of the chemical composition of the cell, particles which are adjacent in physical space will interact with one another by mixing. Mixing models like those shown in the next chapter can represent the physical mixing within the cell. However, in order for the mixing models to work, adjacent particles need to be found, a task which is either computationally expensive, memory intensive or a combination of both, depending on the underlying algorithms.

4.5 Joint Presumed Discrete Distributions (jPDD)

The present work combines ideas from both approaches, as it employs multivariate ensembles of discrete particles to represent Filtered Density Functions (as in transported PDFs), but generates those ensembles using transport equations for statistical moments (as in presumed PDF). Those FDFs provide a closure for the chemical source term and are used to model the sub-grid scale mixing state of each cell. The particle ensembles (or *distributions*) are herein defined by their first and second order statistical moments. This so called joint probability discrete distribution (or jPDD) approach has been suggested previously for the Reynolds-Averaged-Navier-Stokes (RANS) context [Bra05, BGP04, BP02, BPI$^+$03]. Brandt et al have employed the jPDD approach sucessfully for combustion processes. In this work, the jPDD approach is refined, adapted for LES and validated using DNS data. A comparison between the three PDF methods is given in table 4.1

Property	presumed	jPDD	transported
Transported items	Moments	Moments	Particles
Mixing process	dissipation rates	dissipation rates & mixing model	mixing model
Coupling	N/A	low	high
Plausibility	low	medium	high
Multiple fractions	limited	several	arbitrary
Computational effort	very low	low	very high
Memory requirement	very low	high	very high

Table 4.1: This table compares the three PDF methods.
Coupling displays the link between the flow field and the probability distribution. Plausibility shows how much other physical properties determine the shape of the distribution

4.6 Transport Equations for PDFs

Previously in this chapter, various types of PDF have been introduced. In order to be able to employ these PDFs within CFD, it is required to derive a transport equation for this PDF. This section will first introduce a general transport equation for a PDF and then derive the transport equation used in this work, which are based on transport equation for statistical moments known from presumed PDF methods.

4.6.1 Transport Equation for a Joint PDF

Fox [Fox03] shows methods how a transport equation for the PDFs can be derived. A transport equation for the full velocity, composition PDF can be derived as

$$\frac{\partial f_{u_i,\phi}}{\partial t} + V_i \frac{\partial f_{u_i,\phi}}{\partial x_i} = -\frac{\partial}{\partial V_i}\left(f\,\langle A_i|V_i,\psi\rangle\, f_{u_i,\phi}\right) - \frac{\partial}{\partial \psi_i}\left(f\,\langle \Theta_i|V_i,\psi\rangle\, f_{u_i,\phi}\right) \quad (4.12)$$

where V_i is the sample space vector. Evolution of the PDF described in equation (4.12) can happen by three main mechanisms

- Convection by the velocity field
- Convection through the conditional acceleration term, which is the first term on the right hand side
- Reaction or Diffusion, which is the second term of the right hand side

The two terms on the right hand side are referred to as *conditional fluxes*. These terms need to be closed, which is done by deriving them from the right hand side of the momentum equation and scalar transport equation, giving

$$\langle A_i|V_i,\psi\rangle = \left\langle \left(\nu \frac{\partial^2 u_i}{\partial x_j^2} - \frac{1}{\rho}\frac{\partial p}{\partial x)i} \right) |V_i,\psi \right\rangle - \frac{1}{\rho}\frac{\partial p}{\partial x_i} + g_i \quad (4.13)$$

and

$$\langle \Psi|V,\psi\rangle = \left\langle \Gamma \frac{\partial^2 \phi_\alpha}{\partial x_j^2} |V_i,\psi \right\rangle + S_\alpha(\psi). \quad (4.14)$$

The first term on the right hand side of both equations are unclosed and are the result of the density/pressure fluctuations and molecular diffusion, respectively. Modeling these terms pose the principal challenge for transported PDF methods.

4.7 Transport Equations for Statistical Moments

As seen in the previous section, transport equations for PDFs contain considerable modeling effort due to unclosed conditional terms. However, as the present work requires transport equations for statistical moments of distributions, these are derived from the basic filtered scalar transport equation. The transport equation for the mean (i.e. filtered value) has already been covered in chapter 2, hence this section will focus on the second order moments.

4.7.1 Scalar Variance

Starting from the basic transport equation of the mixture fraction in LES context, using an eddy diffusivity model

$$\frac{D\overline{f}}{Dt} = (\Gamma + \Gamma_{SGS}) \frac{\partial^2 \overline{f}}{\partial x_j \partial x_j}, \tag{4.15}$$

the transport equation for the sub-grid scale scalar variance $\overline{f'^2}$ can be derived.

If the sub-grid scale scalar variance are the subgrid scale fluctuations, thus

$$\overline{f'^2} = \overline{(f - \overline{f})^2}, \tag{4.16}$$

which, by restricting the allowable filter operations to projectors, simplifies to [JDCB01]

$$\overline{f'^2} = \overline{f^2} - \overline{f}^2. \tag{4.17}$$

Using the definition of the *filtered density function* introduced earlier in chapter 4, the second order moment, which is the sum of the square of fluctuations about the filtered values yields [GO93, DVnF97]

$$\int \left[\Gamma - \overline{f(x_i)}\right] \overline{P}(\Gamma, x_i) d\Gamma = \overline{f^2(x_i)} - \overline{f(x_i)}^2. \tag{4.18}$$

Deriving the full transport equation for the scalar variance then results, with $\overline{V}_f = \overline{f'^2}$ in [JDCB01]

$$\begin{aligned} \frac{\partial \overline{V}_f}{\partial t} + \frac{\partial \overline{u_i} \overline{V}_f}{\partial x_i} =& \Gamma \frac{\partial^2 \overline{V}_f}{\partial x_i^2} - 2\Gamma \overline{\frac{\partial f}{\partial x_i} \frac{\partial f}{\partial x_i}} + 2\Gamma \frac{\partial \overline{f}}{\partial x_i} \frac{\partial \overline{f}}{\partial x_i} \\ & - \frac{\partial \overline{u_i f^2} - \overline{u_i}\,\overline{f^2}}{\partial x_i} + 2\overline{f} \frac{\partial \overline{u_i f} - \overline{u_i}\,\overline{f}}{\partial x_i}. \end{aligned} \tag{4.19}$$

Using a typical eddy diffusivity approach for the last two terms on the right hand side of equation (4.19), which represent transport of the scalar field by the sub-grid scale turbulence, gives the transport equation with only a single unclosed term

$$\begin{aligned}\frac{\partial \overline{V}_f}{\partial t} + \frac{\partial \overline{u_i}\overline{V}_f}{\partial x_i} =& (\Gamma + \Gamma_{SGS})\frac{\partial^2 \overline{V}_f}{\partial x_i^2} + 2(\Gamma + \Gamma_{SGS})\frac{\partial \overline{f}}{\partial x_i}\frac{\partial \overline{f}}{\partial x_i} \\ & - 2\Gamma\overline{\frac{\partial f}{\partial x_i}\frac{\partial f}{\partial x_i}}.\end{aligned} \tag{4.20}$$

Note that for large Reynolds numbers the sub-grid scale diffusivity Γ_{SGS} far outweighs the molecular diffusivity Γ. As shown in chapter 2, Γ_{SGS} can be determined using a dynamic scheme, reducing the number of fixed model constants.

This term,

$$\overline{\chi} = 2\Gamma\overline{\frac{\partial f}{\partial x_i}\frac{\partial f}{\partial x_i}}, \tag{4.21}$$

is known as the *scalar dissipation rate* and referenced to as $\overline{\chi}$ in this work, requires another closure approach. The scalar dissipation rate is the main mechanism that reduces sub-grid scale scalar variance, due to the quadratic nature of the term. Also, note that scalar variance is mainly reduced where the gradient of the mean field is high. Modeling this term has been a very active field or research recently especially in RANS context, where it has been found to have a high influence on the reaction rate in turbulent reacting flows at high Damköhler numbers.

4.7.2 Closure for the Scalar Dissipation Rate

It has been suggested [PM98] to assume that the scalar dissipation and the variance production are in equilibrium, as in

$$\overline{\chi} = 2\Gamma\overline{\frac{\partial f}{\partial x_i}\frac{\partial f}{\partial x_i}} = 2(\Gamma + \Gamma_{SGS})\frac{\partial \overline{f}}{\partial x_i}\frac{\partial \overline{f}}{\partial x_i}. \tag{4.22}$$

In a closed system, the total amount of variance would thus be constant, while mixing is a process that is known to reduce variance [MJ06]. This assumption has been used in a context where no transport equation for the variance was present.

If a variance transport equation is employed, however, a model for the scalar dissipation rate is required that reduces scalar variance during the mixing process.

As such, Jimenez et al [JDCB01] have suggested a non-equilibrium approach that models the scalar dissipation rate using the mechanical–to–scalar time scale ratio, thus

$$\overline{\chi} = C_R V_f \overline{\tau}_f, \tag{4.23}$$

with τ_f as the characteristic mixing time. The same author also determines the modelling parameter C as

$$C_R = \frac{1}{\mathrm{Sc}} \tag{4.24}$$

taken from an a priori analysis of DNS data. By approximating the characteristic mixing time as the ratio between kinetic energy $\overline{\kappa}$ and the kinetic energy dissipation $\overline{\varepsilon}$, it can be written as

$$\overline{\tau_f} = \frac{\overline{\kappa}}{\overline{\varepsilon}}. \tag{4.25}$$

Unless a $k-\varepsilon$ model is used to model the turbulence, values for $\overline{\kappa}$ and $\overline{\varepsilon}$ need to be obtained from available values, for example by using a Smagorinsky-type approach for the dissipation rate $\overline{\varepsilon}$ [Sma63] and a Yoshizawa approach for the kinetic energy $\overline{\kappa}$ [YH85], resulting in

$$\overline{\tau_f} = \frac{\overline{\kappa}}{\overline{\varepsilon}} = \frac{2C_I\overline{\Delta}^2\overline{S}_{ij}\overline{S}_{ij}}{2\left(\nu + C_S\overline{\Delta}^2\left|\overline{S}\right|\right)\overline{S}_{ij}\overline{S}_{ij}}. \tag{4.26}$$

Fox [Fox03] shows that at Schmidt numbers of around unity the mechanical-to-scalar time-scale ratio will be approximately constant, $\tau_f \approx 2$, for a given Taylor-scale Reynolds number.

Combining equation (4.23) with equation (4.26) yields the model equation for the scalar dissipation rate as [FP10]

$$\overline{\chi} = \frac{\nu + C_S\overline{\Delta}^2\left|\overline{S}\right|}{\mathrm{Sc}\,C_I\overline{\Delta}^2}\left(\overline{f^2} - \overline{f}^2\right). \tag{4.27}$$

4.7.3 Scalar Covariance

As was shown in section 3.4.2, the covariance is a generalization of the variance, in other words, the variance is the covariance of a statistical variance with itself. This yields the transport equation for the covariance as

$$\begin{aligned}\frac{\partial \overline{C}_{f_1 f_2}}{\partial t} + \frac{\partial \overline{u_i}\overline{C}_{f_1 f_2}}{\partial x_i} =& \Gamma \frac{\partial^2 \overline{C}_{f_1 f_2}}{\partial x_i^2} - 2\Gamma \overline{\frac{\partial f_1}{\partial x_i}\frac{\partial f_2}{\partial x_i}} + 2\Gamma\left(\frac{\partial \overline{f}_1}{\partial x_i}\right) + 2\Gamma\left(\frac{\partial \overline{f}_2}{\partial x_i}\right) \\ & - \frac{\partial \overline{u_i f_1 f_2} - \overline{u_i}\,\overline{f_1 f_2}}{\partial x_i} + \overline{f}_2 \frac{\partial \overline{u_i f_1} - \overline{u_i}\,\overline{f}_1}{\partial x_i} + \overline{f}_1 \frac{\partial \overline{u_i f_2} - \overline{u_i}\,\overline{f}_2}{\partial x_i}.\end{aligned} \tag{4.28}$$

For a detailed derivation of this, see the appendix A.

When employing the same models as for the variance this leads to

$$\begin{aligned}\frac{\partial \overline{C}_{f_1 f_2}}{\partial t} + \frac{\partial \overline{u_i}\overline{C}_{f_1 f_2}}{\partial x_i} =& (\Gamma + \Gamma_{SGS}) \frac{\partial^2 \overline{C}_{f_1 f_2}}{\partial x_i^2} + 2(\Gamma + \Gamma_{SGS}) \frac{\partial \overline{f}_1}{\partial x_i}\frac{\partial \overline{f}_2}{\partial x_i} \\ & - 2\Gamma \overline{\frac{\partial f_1}{\partial x_i}\frac{\partial f_2}{\partial x_i}},\end{aligned} \tag{4.29}$$

with the unclosed term

$$\overline{\chi}_{12} = 2\Gamma \overline{\frac{\partial f_1}{\partial x_i}\frac{\partial f_2}{\partial x_i}}, \tag{4.30}$$

remaining. This is called the *scalar cross dissipation rate*. It should be noted that this term is no longer quadratic in nature like the scalar dissipation rate is. Thus, it is a mechanism that can both produce and remove scalar covariance.

4.7.4 Closure for the Cross Dissipation Rate

Using the same approach as in section 4.7.2 the resulting model for the scalar cross-dissipation rate reads

$$\overline{\chi}_{12} = \frac{\nu + C_S \overline{\Delta}^2 \left|\overline{S}\right|}{\mathrm{Sc} C_I \overline{\Delta}^2} \left(\overline{f_1 f_2} - \overline{f_1}\,\overline{f_2}\right). \tag{4.31}$$

4.7.5 The Full Set of Transport Equations

This is the complete set of transport equations required for the incompressible LES solver using means, variances and covariance for the mixture fractions.

- Continuity equation

$$\frac{\partial \overline{u}_i}{\partial x_i} = 0. \tag{4.32}$$

- Momentum equation

$$\frac{\partial \overline{u}_i}{\partial t} + \overline{u}_j \frac{\partial \overline{u}_i}{\partial x_j} = \nu \frac{\partial^2 \overline{u}_i}{\partial x_i^2} - \frac{\partial \overline{p}}{\partial x_i} - \frac{1}{\rho} \frac{\partial \tau_{ij}}{\partial x_j} \tag{4.33}$$

- Transport equation for the mean of the mixture fraction

$$\frac{\partial \overline{f}_i}{\partial t} + u_j \frac{\partial \overline{f}_i}{\partial x_j} = (\Gamma + \Gamma_{SGS}) \frac{\partial^2 \overline{f}_i}{\partial x_i^2} \tag{4.34}$$

- Transport equation for the variance of the mixture fraction

$$\begin{aligned} \frac{\partial \overline{V}_{f_i}}{\partial t} + \frac{\partial \overline{u_i} \overline{V}_{f_i}}{\partial x_i} = (\Gamma + \Gamma_{SGS}) \frac{\partial^2 \overline{V}_{f_i}}{\partial x_i^2} + 2(\Gamma + \Gamma_{SGS}) \frac{\partial \overline{f}_i}{\partial x_i} \frac{\partial \overline{f}_i}{\partial x_i} \\ - \frac{\nu + C_S \overline{\Delta}^2 |\overline{S}|}{\mathrm{Sc} C_I \overline{\Delta}^2} \left(\overline{f_i^2} - \overline{f}_i{}^2 \right) \end{aligned} \tag{4.35}$$

- Transport equation for the covariance of the mixture fractions

$$\begin{aligned} \frac{\partial \overline{C}_{f_1 f_2}}{\partial t} + \frac{\partial \overline{u_i} \overline{C}_{f_1 f_2}}{\partial x_i} = (\Gamma + \Gamma_{SGS}) \frac{\partial^2 \overline{C}_{f_1 f_2}}{\partial x_i^2} + 2(\Gamma + \Gamma_{SGS}) \frac{\partial \overline{f}_1}{\partial x_i} \frac{\partial \overline{f}_2}{\partial x_i} \\ - \frac{\nu + C_S \overline{\Delta}^2 |\overline{S}|}{\mathrm{Sc} C_I \overline{\Delta}^2} \left(\overline{f_1 f_2} - \overline{f_1}\,\overline{f_2} \right) \end{aligned} \tag{4.36}$$

With

$$\tau_{ij} = -2\left(C_S\Delta\right)^2 \left|\overline{S}\right| \overline{S}_{ij} \tag{4.37}$$

$$\Gamma_{SGS} = \frac{2\left(C_S\Delta\right)^2}{Sc_{SGS}} \left|\overline{S}\right| \tag{4.38}$$

$$\left|\overline{S}\right| \equiv \left(2\overline{S}_{ij}\overline{S}_{ij}\right)^{\frac{1}{2}} \tag{4.39}$$

$$\overline{S}_{ij} \equiv \frac{1}{2}\left(\frac{\partial u_i}{\partial x_j} + \frac{\partial u_j}{\partial x_i}\right). \tag{4.40}$$

Note: Using a dynamic procedure for C_I and C_S fully closes this system of equations.

5 A Priori Validation of Model Assumptions

This chapter will assess the quality of the developed model against DNS data. The first section of this chapter, 5.1 will explain how each model assumption will be tested against DNS data. The following section, 5.2 explains the physical configuration of the test up and the rationale behind selecting it. Section 5.3 then introduces the CFD solvers used and the numerical setup of the computations. After that, section 5.4 explains the post-processing of the DNS data that is required to validate the model.

5.1 Validation Strategy

Three questions need to be answered when judging the quality of the model developed for this work.

1. The transport equations developed in chapter 4 contain a number of unclosed terms, for which models have been devised. Such equations have been developed for the first and second order statistical moments of the distribution. The first order moment represents the mean of the distribution. In this case, a standard eddy-diffusivity approach with dynamic model closure has been employed. This method has been used widely in the past for both academic research and technical applications.

   Thus, the validation effort for the transport equations focuses on the transport equations for the second order moments, which represent the variances and covariance of the distribution. Here, the crucial part is the modeling of the *scalar dissipation rate* in the variance transport equation and the *scalar cross dissipation rate* in the covariance transport equation. The results of this analysis are shown in section 5.5.

2. The jPDDs generated by the mixing model are used to compute reaction rates. Thus, the reaction rates need to be validated by being compared to DNS data. However, there are no such distributions in DNS. It is therefore required to devise a scheme that extracts distributions from DNS computations. These *DNS distributions* are then used to compute a DNS reaction

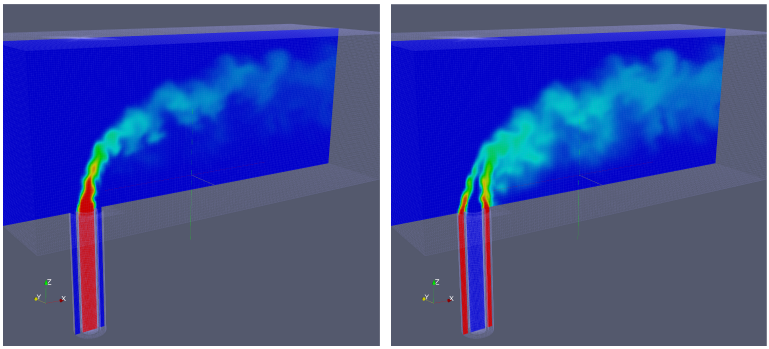

(a) Mixture fraction of central jet **(b)** Mixture fraction of annular jet

Figure 5.1: DNS of a co-annular jet-in-crossflow, showing the mixture fractions for the two jets, main flow from left to right. (a) Mixture fraction of central jet. (b) Mixture fraction of annular jet.

rate, which is compared against the one obtained from the jPDD. The results from this comparison are discussed in section 5.6.

3. In this work, jPDDs of two mixture fractions are characterized by five parameters: two mean values, one for each mixture fraction, two variances and the covariance. The question that arises is whether those five parameters are sufficient or whether others shall be taken into account. Natural candidates for additional parameters were the scalar dissipation rates and the scalar cross dissipation rate. In order to answer this question, the DNS data has been filtered again. However, this time the extraction of distributions from DNS data was performed so that the DNS distributions were not only defined by the five model parameters but also by additional parameters. The dependence of the reaction rate on the additional parameters could then be assessed. These dependencies are shown in section 5.7.

5.2 Validation Configuration

The validation platform from the presented model is the co-annular jet-in-crossflow arrangement. This arrangement differs from the normal jet-in-crossflow

arrangement by the fact that the jet which enters the main flow consists of two jets itself. The standard circular jet is enveloped by an annular jet, with each jet carrying an own mixture fraction. A representation of such a flow can be seen in figure 5.1, where the two mixture fractions of the jets can be seen.

This configuration has been chosen for three reasons. First of all, it resembles, in a simplified manner, the configuration of the SEV burner in the Alstom gas turbine (cf. figure 1.1) that has been the inspiration of this entire work. Furthermore, an experimental configuration of a co-annular jet-in-crossflow arrangement was planned. Finally, the single jet-in-crossflow serves as a basis of understanding mixing processes in the CFD community and also within the SPP1141.

5.3 Solvers and Setup

In this thesis, two different solvers have been used to perform DNS: MGLET, which was started under the supervision of Wengle [WW89] and is currently being developed by the group of Prof. Manhart at the Technische Universität München [Man04, MTF01], and alternatively OpenFOAM, which is an open source CFD solver with a large and growing community. Two solvers have been used as their properties complement each other well. In order to perform the simulations, two clusters were available. First, the Lehrstuhl für Thermodynamik had its own compute cluster for medium sized simulations. On the other hand, large simulations have been performed on the 64bit cluster of the Leibniz Rechenzentrum (LRZ) in Munich, Germany.

5.3.1 MGLET

MGLET is a FORTRAN77 based, high performance solver for incompressible flows which uses a Cartesian staggered grid approach. In order to perform the simulations needed for this thesis, it was required to extend MGLET's capability from a single passive scalar to multiple scalars. This extension has been implemented as an external C library, which plugs into the MGLET solver instead of the previous single-scalar capability. MGLET has been used in this thesis for a number of simulations with simple geometries and for simulations with higher Reynolds numbers, due to its considerable speed advantage over OpenFOAM. Apart from a number of tests for the implementation of the multiple scalar transport equations, one of the benchmark computations was a moderate Reynolds number channel

with a co-annular jet-in-crossflow configuration with the following parameters:

Parameter	high Re number	low Re number
Maximum velocity of main flow	1.0	1.0
Channel height	2.0	0.4096
Viscosity	0.000355	0.0001138
Reynolds number (half channel)	2817	1800
Channel length	4.8	0.72
Diameter of outer jet	1.0	0.12
Reynolds number (jet diameter)	2817	1054
Maximum velocity of jets	3.0	3.0
Reynolds number (jet)	2112	780
Grid dimensions	350x144x128	256x200x256
Grid points	6451200	13107200
Schmidt number	1	1
Number of CPUs	2	4

All values are in their respective SI $[m, kg, s]$ units for this and all subsequent tables. A second simulation was performed at a considerably higher Reynolds number with a smaller jet, where only the near-field of the influx location was simulated. It can be noted that the flow with the lower Reynolds number actually has a higher number of grid points. This is due to the fact that for the low Reynolds number computation, an equidistant grid was used. However, in large sections of the channel, especially further downstream and near the wall opposite of the jet, the number of points exceeded the requirement for a DNS. For the higher Reynolds number flow, a non-equidistant grid has been used, which reduced the very large number of grid points compared to a non-equidistant grid. Both simulations used a second order central difference scheme for the spatial discretization with a 3rd order Runge-Kutta time step scheme. An example of such a flow computation in MGLET is displayed in figure 5.2

Note that in these computations, the inflow pipes of the channel were not simulated. Instead, the co-annular jet was set up as a simple boundary condition on the bottom wall with a cosine-shaped velocity profile. This lead to some numerical instabilities. Due to the fact that the value of the scalar changes from 0 to 1 within a single cell, the employed second order central difference scheme will lead to out-of-bounds data for the scalar as can be seen in figure 5.3.

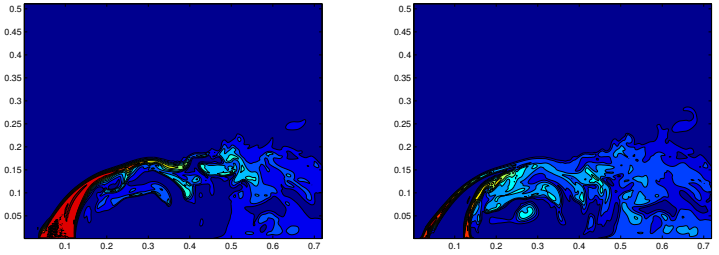

Figure 5.2: DNS computation from MGLET, using 256x200x256 grid points,with one scalar shown on the left and the second scalar, corresponding to the annular jet, on the right. Main flow from left to right.

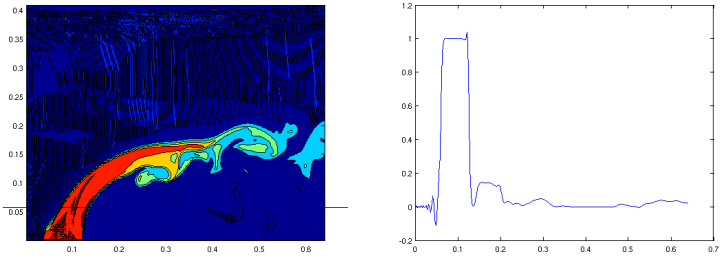

Figure 5.3: DNS of a jet-in-crossflow arrangement. Left is the two dimensional plot along the center of the channel, right is the one dimensional plot of the scalar along the line indicated on the left side. The out-of-bounds values can be seen clearly

5.3.2 OpenFOAM

OpenFOAM is a CFD software suite with a large and growing community, both in academic and commercial environments. For the DNS simulations, the so called "oodles" solver has been used, an incompressible LES solver which supports a number of discretization and time stepping schemes. For the present work, it was required to implement scalar transport equations into the solver. OpenFOAM, despite its considerably lower absolute performance, has been used in this work because of several advantages it offered of MGLET in some areas:

- OpenFOAM is written in heavily templated C++, offering very fast development and testing. It is only required to formulate the equation and all the discretization, etc. will be done by the underlying system. The ease of implementing transport equations in OpenFOAM can be seen in appendix C,which shows the full implementation of the transport equations used in this thesis.
- It supports unstructured grids. For the co-annular jet-in-crossflow, a full geometry including inlet pipes has been set up using a commercial grid generator (ANSYS ICEM).

As seen previously, not simulating the inflow pipe of the jet leads to non-physical values of the scalars.Thus, for OpenFOAM computations, a grid was created that also contains a section of the inflow pipes. An example of the geometry used for the OpenFOAM computations using a full co-annular jet-in-crossflow arrangement has been shown previously in figure 5.1. At the inflow plane, a uniform velocity has been set as boundary condition. The velocity profile halfway through the pipes can been seen in figure 5.4.

The solver setup for the OpenFOAM DNS has been:

Parameter	Value
Maximum velocity of main flow	0.355
Channel height	0.06
Viscosity	0.00000355
Reynolds number (half channel)	3000
Channel length	0.15
Diameter of outer jet	0.012
Reynolds number (jet diameter)	1200
Maximum velocity of jets	1
Reynolds number (jet)	1600
Grid points	2082600
Schmidt number	1
Number of CPUs	64

Comparing the two solver setups, in particular the number of CPUs required, shows the significant performance advantage the MGLET solver enjoys over OpenFOAM.

In OpenFOAM an unstructured grid has been used, with most of the cells clustered around the entry points of the jets. The pipes have been meshed using an O-grid approach, which extends to the opposite (top) wall of the main channel. The main channel itself has been meshed using a conventional, structured grid. In order to assess the quality of the DNS grid, i.e. whether the resolution is sufficient, a test simulation with an activated LES model has been performed. The sub-grid scale viscosity of this simulation is shown in figure 5.5. It can be seen that the sub-grid scale viscosity is, throughout the domain, more than an order of magnitude smaller than the molecular diffusion. Thus, the resolution used for the DNS is sufficient.

The Schmidt number of the flow is unity, so that the Batchelor-length scale is identical to the Kolmogorov-length scale (cf. equation (2.58). The resolution of the DNS is then selected to be sufficient to eliminate scalar sub-grid scale fluctuations, thus the DNS cells contain no scalar variance or co-variance. Transport equations for two mixture fractions have been solved. One mixture fraction is set to unity for the central jet, the other for the annular jet.

5.4 Post-processing of DNS Data

One part of the validation strategy is to assess the reaction rates that are obtained from the jPDDs by comparing them against DNS data. In a further validation step,

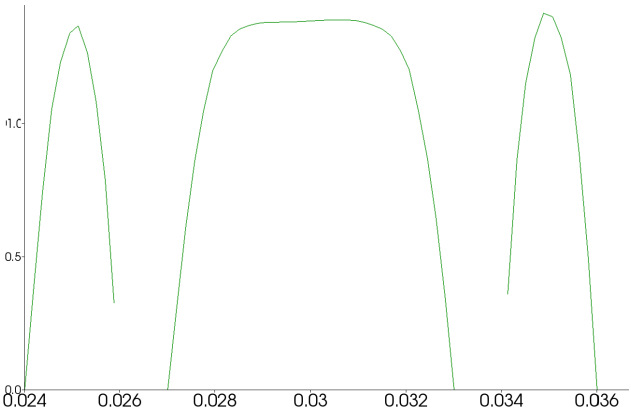

Figure 5.4: Velocity profile in the inlet pipes of a co-annular jet-in-crossflow configuration, after half the length of the pipe

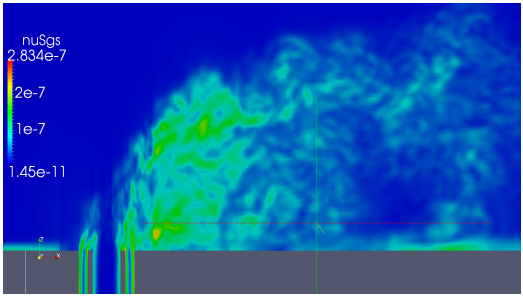

Figure 5.5: Sub-grid scale viscosity of an LES test run using a DNS grid to assess the resolution of the grid. The molecular viscosity of the computation is 3.55e-6. It can been seen that the contribution of the sub-grid scale model is between one and two orders of magnitude lower than the molecular viscosity, showing that the resolution of the DNS is sufficient

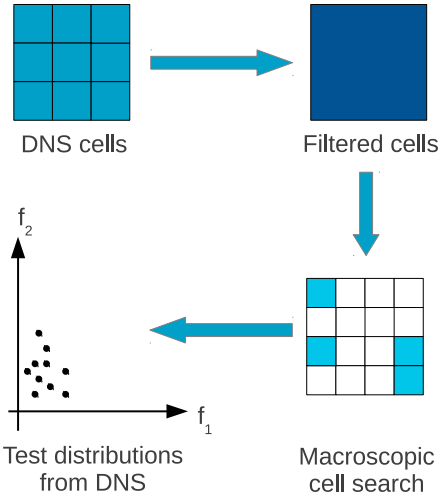

Figure 5.6: The filtering and sweep process to obtain test distributions for comparison with the mixing model.
Step 1: A coarser grid is superimposed onto the DNS grid creating small distributions.
Step 2: Small distributions with similar statistical moments are sought throughout the domain both in spatial and temporal dimensions.
Step 3: Similar distributions are put together into one macroscopic distribution.

it should be determined whether the first and second order moments are indeed sufficient to characterize the mixing state. However, each cell in the DNS has only one sample of mixture fractions, as there is no variance within the computational cell. The following scheme, which is depicted in figure 5.6 has been developed to obtain distributions from the DNS data:

1. A test grid is generated that has a significantly lower resolution than the computational grid for the DNS. For the Cartesian grids in the MGLET simulations, the test grid was between three and eight times coarser than the computational grid. Hence, each cell in the test grid contains between 27 and 512 samples of mixture fractions.

2. For each cell in the test grid, statistical moments of the distributions within the test grid are computed.

3. The number of samples in each of the test grid cell is still too low (27 to 512) to provide reliable statistics. Hence, all test grid distributions that possess the same first and second order moments, within a certain margin of error, are combined into a single distribution with a large number of same, called *DNS distribution*. The search for similar cells can be performed in all spatial and the temporal dimension to maximize the number of sample for the macroscopic distributions.

In the scheme explained above, distributions that possess the same first and second order moments are combined. The set of parameters according to which the combination is performed is called *clustering parameters*. The scheme was developed so that any variable that is available at a test grid cell can be used as clustering parameter.

For the first part of the validation, which is the comparison of reaction rates obtained from jPDDs and DNS distributions, five clustering parameters have been selected.

- The mean value of both mixture fractions
- The variances of both mixture fractions
- The correlation of the mixture fractions

In the second part of the validation of jPDDs, the question arises whether these 5 parameters are sufficient to characterize the distribution, or whether other parameters of the distribution, or the flow, play a major role in the resulting reaction rates. To answer this question, the set of clustering parameters has been extended by

- the scalar dissipation rate of either scalar.
- the scalar cross-dissipation rate.
- any combination of dissipation rates and cross dissipation rates.

Within this post processing scheme, three things are of interest. First, as the underlying computation is a DNS, the dissipation rates are not readily available. However, using the modeling approach as shown in chapter 4, it is possible to compute scalar dissipation rates for the test grid cells using the flow parameters.

Second, using all the additional parameters to characterize the distributions results in an 8-dimensional[1] problem. "Typical" regions in this 8-dimensional state

1 two means, two variances, two dissipation rates, one covariance and one cross dissipation rate

space will have a large number of samples associated to them. However, the extremes of the state space will most likely have very few or even no samples as only very few test grid cells are found that have the correct set of clustering parameters. This problem can be mitigated by computing more time steps during the DNS, thus generating a high total number of samples, but this comes at high computational cost.

Finally, while this post processing scheme is applied to the DNS data, all the possible sets of clustering parameters need to be stored. As, from a numerical point of view, no two test grid cells will have exactly the same values for the clustering parameters, a certain amount of difference between the parameters of two test grid cells are allowed. In other words, the total range for each parameter was subdivided into 'bins'. For example, if only a single clustering parameter, for instance the mean mixture fraction, was chosen, all test grid distributions with a value of 0.00 to 0.05 would constitute one DNS distribution. A test grid distributions with a mean mixture fraction value of 0.05 to 0.1 would form a second DNS distribution, from 0.1 to 0.15 a third, and so forth. In this simple scheme, in the end there would be 20 DNS distributions.

However, the problem at hand is multi dimensional. If five clustering parameters are selected, already 3.2 million different 'bins' exist. With all 8 clustering parameters enabled, this number grows to 25.6 billion, rendering this approach useless unless fewer bins are chosen for at least some of the dimensions.

5.5 Post Processing Results

This section will give a brief overview of the results obtained by spatially filtering an instantaneous flow field, as provided by the OpenFOAM DNS solver. Figure 5.7 shows the scalar fields of the two mixture fractions as a visual reference for the following figures.

5.5.1 Variances and Scalar Dissipation Rates

Figures 5.8 and 5.9 show the variances and the scalar dissipation rates of the two mixture fractions, as computed from DNS. Not unexpected, the scalar variance builds up rapidly where there is a steep scalar gradient, which is in accordance with the transport equations for the LES model. Also, the scalar dissipation rate ramps up quickly so that scalar variance decays over the evolution of the flow.

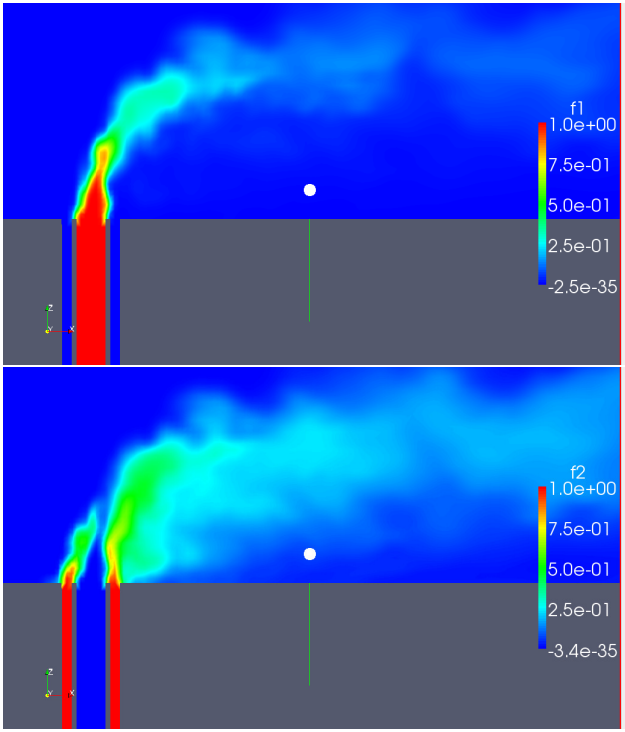

Figure 5.7: Scalar 1 (top) and Scalar 2 (bottom) of a DNS is co-annular jet-in-crossflow arrangement.

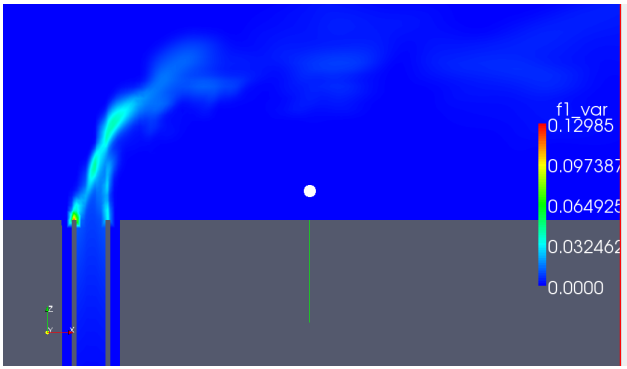

(a) Variance of scalar 1 (central jet)

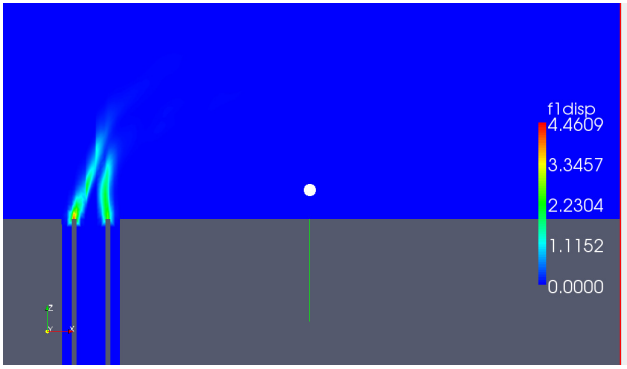

(b) Dissipation rate of scalar 1 (central jet)

Figure 5.8: Stream wise slice of the co-annular jet-in-crossflow. (a) Scalar variance of mixture fraction 1. (b) Corresponding scalar dissipation rate

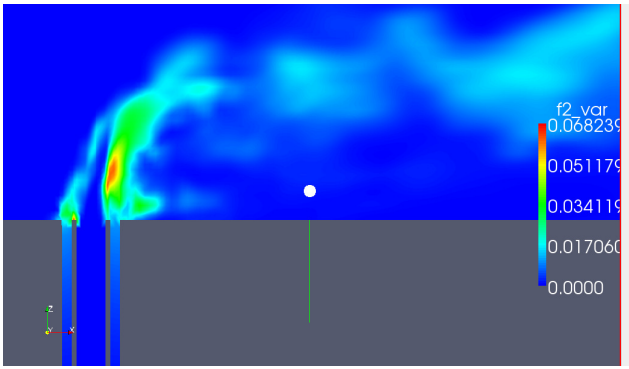

(a) Variance of scalar 2 (annular jet)

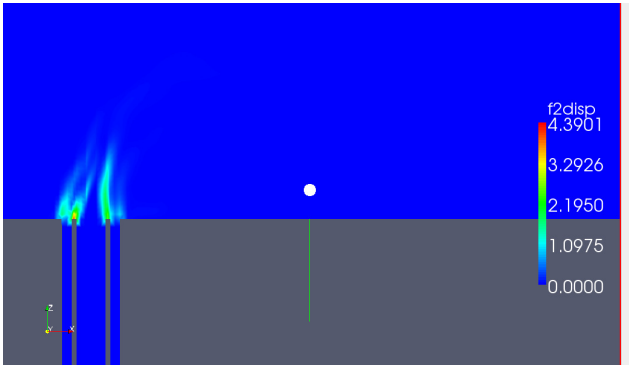

(b) Dissipation rate of scalar 2 (annular jet)

Figure 5.9: Stream wise slice of the co-annular jet-in-crossflow. (a) Scalar variance of mixture fraction 2. (b) Corresponding scalar dissipation rate

5.5.2 Covariance and Scalar Cross Dissipation Rate

Figure 5.10 shows the covariance and the corresponding scalar cross dissipation rate of the two mixture fractions. It can be seen that at the influx, where both mixture fractions enter the main flow, the absolute value of the covariance is at its peak. Also, at the same location the scalar cross dissipation has a high absolute value of the same sign. Very much like the scalar dissipation rate is attempting to remove variance, the scalar cross dissipation is responsible for removing any covariance as the fluid evolves.

It is worth noting that the filtered DNS data shows that within the region of high scalar gradients (cf. figure 5.7), a considerable amount of covariance is present. Figure 3.4 shows that at least for some reactions, the covariance plays a noticeable role. Thus, including the covariance into the calculation will lead to a more accurate prediction of the mixing process and, in extension, the reaction rate of the system.

As for the variances and the covariance, the values shown here are the residual sub-grid scale dissipation rates and cross dissipation rate. As expected, high values of the dissipation rates occur where the variance of the corresponding scalar is high, which is reflected in the LES model as shown in section 4.7.2 and 4.7.4. Scalar dissipation rates are always positive, i.e. the decay the corresponding variance. This is in contrast to the scalar cross dissipation rate, which can be positive or negative, thus it can dissipate as well as produce scalar covariance.

5.5.3 Mechanical to Scalar Time Scale Ratio

Figure 5.11 shows the mechanical-to-scalar time scale ratio of the DNS computation. This ratio, for Schmidt numbers around unity, is assumed to be around 2 for fully developed spectra. As can be seen the time scale ratio varies greatly between zero and values larger than 10. This is due to the fact that the mixing process does not yet possess a fully developed spectrum in the section of the computational area shown.

However, as can be seen in figure 5.12, the largest part of the regions with ratios of zero or over 5 are at places wherethe mixture fraction is zero or near zero. In areas where most of the mixing takes place, the time scale ratio is closed to the expected value of 2. However, further investigation in this matter is needed, as at places where the time scale ratio deviates from 2, the transport equation for the dissipation rate will over- or under predict the mixing.

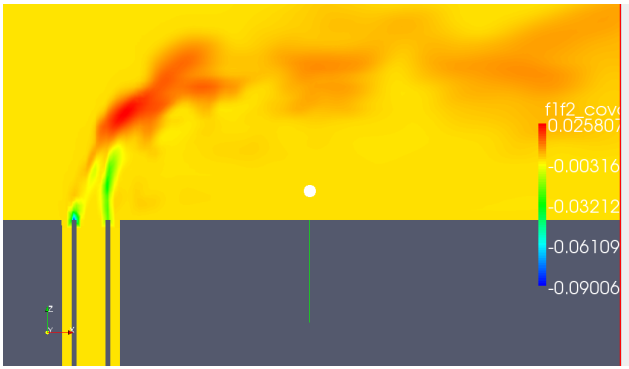

(a) Covariance

(b) Cross dissipation rate

Figure 5.10: Stream wise slice of the co-annular jet-in-crossflow. (a) Covariance of the two mixture fractions. (b) Scalar cross dissipation rate

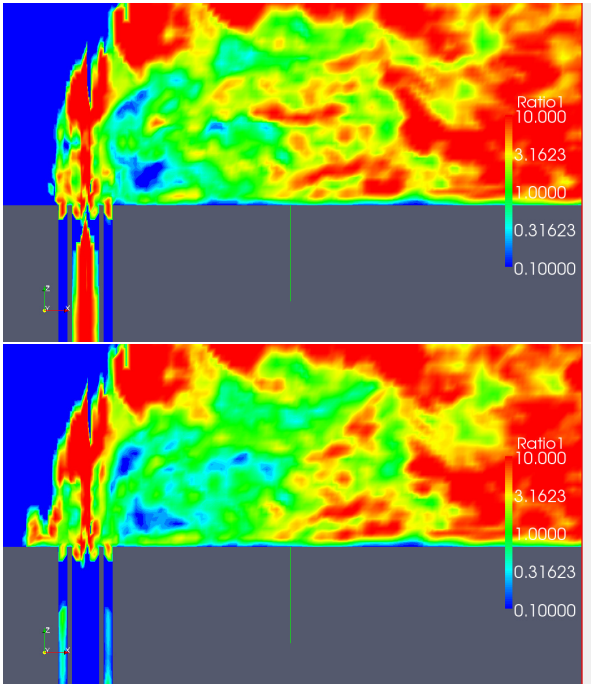

Figure 5.11: Mechanical-to-scalar time scale ratio of scalar 1 (top) and scalar 2 (bottom)

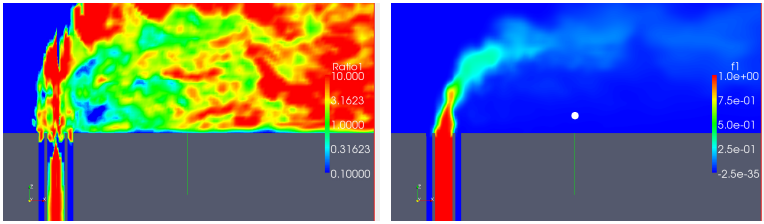

(a) Time scale ratio of scalar 1 **(b)** Mean of scalar 1

Figure 5.12: Side-by-side display of the mechanical-to-scalar time scale ratio and the mean of the same scalar. (a) Mechanical to scalar time scale ratio. (b) mean value of the mixture fraction.

5.5.4 Transport equations

In chapter 4 the transport equations that are required for this model were presented. Those equations contain some unclosed terms that require modeling. In order to assess the quality of this modeling, the corresponding values have been determined for the DNS, and then compared to the LES of the same flow.

For this comparison, an LES of the co-annular jet-in-crossflow configuration has been performed with identical geometrical and flow configuration as in the DNS show insection 5.3. The amount of grid points has been reduced, in this case to around 400000 cells, while the DNS had over 2 million cells. The following models have been used:

- Smagorinsky model (dynamic) for the sub-grid scale stresses
- Eidson model (dynamic) for the sub-grid scale scalar flux
- The model presented in chapter 4 for the scalar dissipation rate and the scalar cross dissipation rate.

In this work, the main terms of the transport equations that required closure were the scalar dissipation rate and the scalar cross dissipation rate. The comparison of the filtered DNS data and the modeled value of the LES for the two scalar dissipation rates are shown in figures 5.13 and 5.14. For scalar 1, i.e. the mixture fraction of the central jet, DNS shows a high scalar dissipation rate around the circular inlet, the LES exhibits a very similar behavior. However, the gradients of the

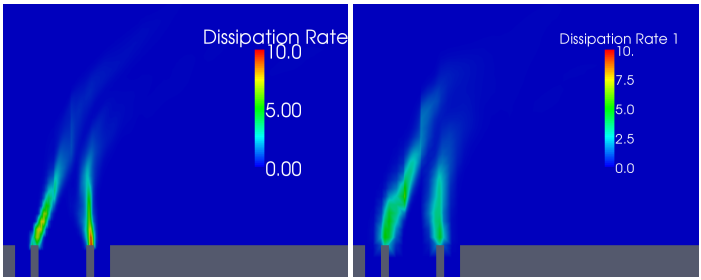

Figure 5.13: Comparison of the sub-grid scalar dissipation rate of scalar 1. Left reference data obtained by filtering DNS, right the LES model

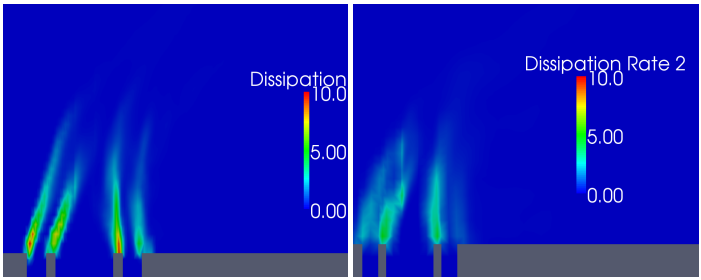

Figure 5.14: Comparison of the sub-grid scalar dissipation rate of scalar 2. Left reference data obtained by filtering DNS, right the LES model

dissipation are more pronounced in the DNS which is a result of the considerably higher grid resolution around the inlet.

For scalar 2, the annular jet, a similar situation occurs. Both LES and DNS compute the scalar dissipation rate near the influx of the jet, however the DNS still has considerable steeper gradients due to the higher grid resolution in the regarded region.

5.6 jPDDs and Reaction Rates

In order to assess the quality of the model, reaction rates are obtained for each cell in the grid, for both the LES and the DNS. As according to chapter 2 the

composition of a DNS cell can be assumed as homogeneous, the LES cells need convolution over the distribution from the model. For an FDF that is represented by particle ensembles, this is the average over the individual reaction rates

$$\overline{\dot{\omega}}\left(\overline{f_1},\overline{f_2},\overline{f_1'^2},\overline{f_2'^2},\overline{f_1'f_2'}\right)=\frac{1}{N}\sum_{i=1}^{N_{part}}\dot{\omega}_i(f_1,f_2). \tag{5.1}$$

The individual reaction rates $\dot{\omega}_i(f_1,f_2)$ can, for example, be obtained using a conventional Arrhenius-like approach, however the model allows any other scheme to be used that computes reaction rates from concentrations. As described before, the first part of the results for the validation of the model copes with the accuracy of the distributions themselves. Distributions that have been obtained from the mixing models are compared against those extracted from DNS by the method described in section 5.4. Figure 5.15 shows this comparison, where the left column shows distributions that have been obtained from the mixing model, and the right column shows those extracted from DNS data. Each row represents a sample set of first and second order moments.

Generally it can be seen that the actual distributions found in a filtered DNS computation and those generated by the model match reasonably well for a variety of first and second order moments. The most noticeable difference can be seen in the set 5.15b, where the model generates a number of artifacts with a high value of the first scalar (the X-axis). In the same set it can also be seen that while the DNS shows a number of points having a zero or near-zero value of the first scalar, these points are missing altogether in the distribution produced by the model. As described before, a mixing model moves all particles towards the mean, dragging them away from the zero-value of the first scalar with each mixing event, thus leaving the gap between the Y axis and the points with the lowest X values. Since the requested mean of the first scalar is rather low, the model requires a number of points with high values of the first scalar to offset the lack of points with low values; this fact leads to the artifacts (few points with values far from the mean of 0.06) that can be seen in the distribution.

Figure 5.16 emphasizes the significance of the covariance. The mixing model is run twice, beginning with the same initial distribution. However, for one run (blue line), the mixing model has been set to establish a correlation of -0.4, while during the second run (green line), a correlation of +0.4 has been produced. After each mixing cycle, the reaction of a sample reaction (in this case, the oxidation of methane) has been computed using an Arrhenius term. As the mixing takes

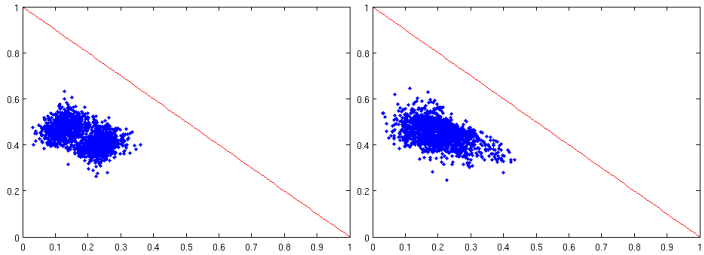

(a) Means: 0.19 and 0.44; Variances: 0.004 and 0.003; Correlation: -0.48

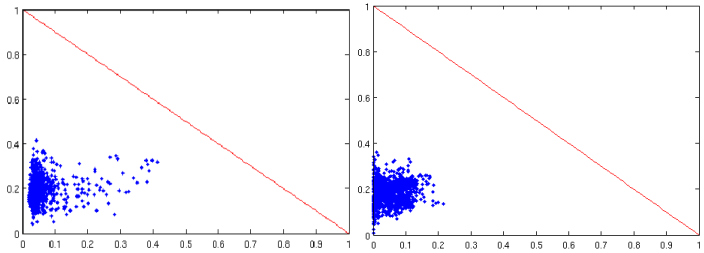

(b) Means: 0.06 and 0.19; Variances: 0.002 and 0.002; Correlation: 0.19

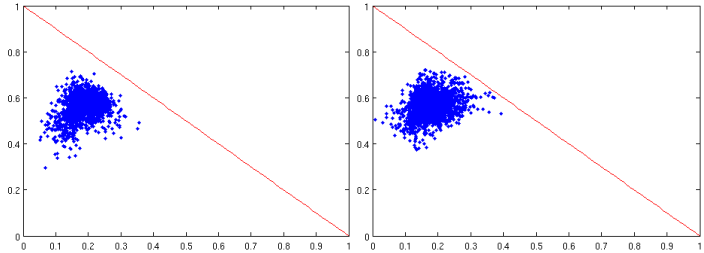

(c) Means: 0.19 and 0.56; Variances: 0.002 and 0.003; Correlation: 0.29

Figure 5.15: Comparison between distributions. Distributions generated by mixing models are displayed in the left column, those taken from the DNS data are shown in the right column. The distributions in one row have the same statistical moments. One scalar fraction depicted on the the X–axis, the other on the Y–axis. Red lines indicate the boundary of the physical space, so that the sum of scalar fractions does not exceed unity. In each case, the resulting reaction rate differs by less than 5%.

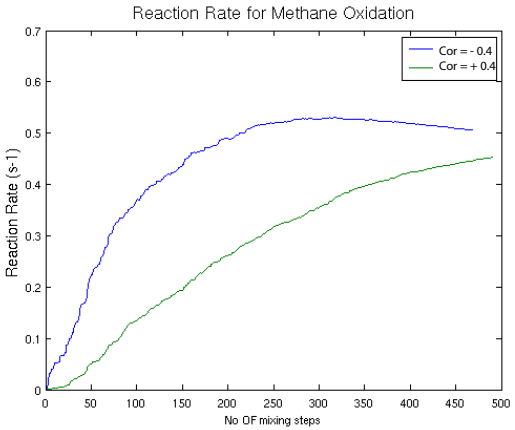

Figure 5.16: Example reaction rate over the number of mixing processes. Means are conserved, Variances decay from left to right. Large differences can be seen between distributions of different correlations. Blue line: negative correlation of -0.4; Green line: positive correlation of +0.4

place, the variance decays for both distributions, however the reaction rates after a given number of mixing events differ greatly between two distributions, although the means are identical and the variances are similar within statistical noise. After a large number of mixing events, the variance is converging towards zero, the covariance subsequently plays a subordinate role.

5.7 Additional Parameters

In section 5.4, it has been explained that numerous test-cells (which are coarser than the actual DNS cells), that have similar first and second order moments, are integrated into a single distribution in order to make the results statistically more meaningful. In Figure 5.17, the individual reaction rates for each of those test cells within a sample distribution (the distribution itself is seen in Fig. 5.17a) are shown. In order to collocate the test-cells, a certain tolerance was applied with respect to the means and variances to allow grouping (as no two cells have

absolutely identical moments). Computing a mean filtered concentration function M with

$$M = f_1^{[\alpha]} f_2^{[\beta]}, \tag{5.2}$$

the concentrations and the Arrhenius-exponents, and comparing this mean concentration function against the filtered reaction rate, as shown in Figure 5.17e, reveals that the deviation of the means of the individual test cells is still paramount to the reaction rate, as a clear dependence can be seen. Figs. 5.17b and 5.17c show the dependency of the reaction rate on the scalar dissipation rates of the first and second scalar, respectively. No dependency between those parameters can be seen. Also the reaction rate does not seem to depend directly on the scalar cross dissipation rate 5.17d. At first, this appears to be in direction contradiction to established theories [Pet84]. However, two points should be taken into account

- In LES, only a part of the scalar dissipation rate actually appears in the model, the sub-grid scale component, as only the sub-grid scale variance is transported. Large amounts of the fluctuations are directly resolved by the grid and thus computed.
- The selected case of auto-ignition in a gas turbine burner is exceptionally slow chemistry, while the typically seen dependence of the reaction rate on the scalar dissipation rate is especially pronounced in fast chemistry systems. Only in fast chemistry small scale reactive-diffusive structures can develop, where the correlation between the reaction rate and the scalar dissipation rate most significant.

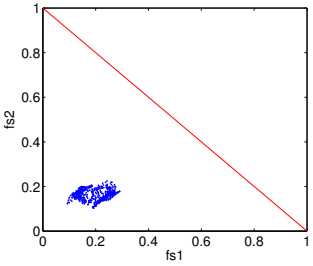

(a) The example distribution

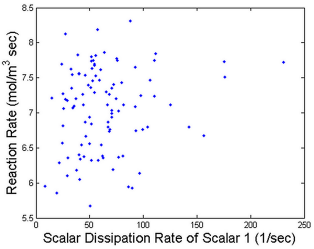

(b) Dependency of the reaction rate on the first scalar dissipation rate

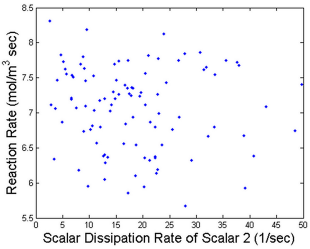

(c) Dependency of the reaction rate on the second scalar dissipation rate

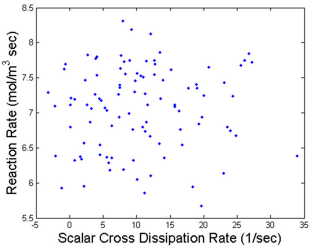

(d) Dependency of the reaction on the scalar cross-dissipation rate

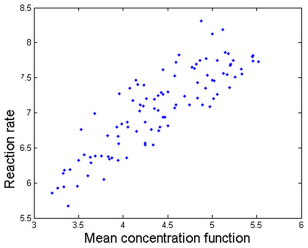

(e) Dependency on the filtered concentration function

Figure 5.17: Reaction rate dependency for a given distribution.

6 Conclusions and Outlook

Within this thesis, an LES model for ternary mixing has been developed, implemented and validated. Chapter 2 presented the theoretical foundation, whereas chapter 3 showed the basics of mixing models and the specific adaptation for this thesis. Chapter 4 then introduced PDF methods and derived the associated transport equations required for this work, along with the sub-grid scale models that are needed for closure. The final chapter 5 then explained the DNS that have been performed as a basis of validation and the results for the validation of the model.

- An offline modeling scheme was developed to store the reaction rates of a chemical system for a mixture fraction based approach. The reaction rates are stored in a table beforehand using the first and second order statistical moments of the mixture fractions, which include the covariance. During the LES, the solver can look up the reaction rate in the table using those statistical moments.
- The reaction rates for this table are generated by using an FDF approach where the mixing state is represented by a particle ensemble. The particle ensemble is created using a specialized version of the Modified Curl mixing model, which has the following adaptations:
  - It can process two mixture fraction simultaneously
  - Starting from a configuration of complete unmixedness, it can generate distributions with specific first and second order moments on demand
- A set of transport equations has been implemented for the first and second order moments of multiple mixture fractions. This set of transport equations possesses two important characteristics:
  - The correlation between the mixture fractions is taken into account.
  - There is no equilibrium assumption between sub-grid scalar variance production and dissipation. Production is performed by resolved gradients of the mean scalar field, while the dissipation takes sub-grid effects into account.

- DNS of co-annular jet-in-crossflow configurations have been performed, which served as a basis for validating the LES model.
- A filtering scheme for the DNS data has been developed, which creates distributions much like the ones used for filling the table described earlier. The DNS distributions have been compared to the ones generated by the mixing model.
- The dissipation rates for the variance and covariance rates predicted by the model have been compared to the DNS data.

Validation of the model against DNS data at low-to-medium Reynolds numbers yielded the following results:

- The distributions created by the mixing model are very similar to the ones obtained by filtering DNS data. This is the case for the distributions themselves and the reaction rates that have been computed for those distributions using a simple reaction.
- No correlation could be obtained between the sub-grid scale scalar dissipation rates and the resulting reaction rates using DNS data. The first and second order moments appear to be sufficient to accurately parametrize the reaction rate, at least at the configuration that has been tested (co-annular jet-in-crossflow). It should however be noted that the sub-grid part of the scalar dissipation rate is only a small part of the total dissipation, due to the nature of the LES. This leads to the conclusion that for these Reynolds numbers only 5 parameters[1] are sufficient to obtain accurate reaction rates.

Several items still remain open for future work

- In this thesis, DNS was the main source of validation. While the numerical setup and schemes of DNS are well established, and DNS is widely regarded as a useful tool for validating new models, it has some limitations. First of all, DNS is intrinsically expensive. As such, the number of different setups that can be performed is very low simply due to the lack of processing power available. Also, since the memory consumption grows very rapidly with the Reynolds number, validation is limited to low-to-medium Reynolds number regimes. Thus, the presented model should be further validated in its entirety against both experiments and transported-PDF LES methods. However, setting up experiments for ternary mixing has been difficult in the

1 for two mixture fractions: two means, two variances, one covariance

past, and separate work needs to be put into an experimental setup that can accurately analyze the mixing processing in a co-annular jet-in-crossflow or similar configuration. Within the SPP1141, experimental validation was planned. However, the experimental setup proved challenging. For the simultaneous measurement of two mixture fractions, two tracer substances are required that not only have different excitation frequencies, but also low cross-excitation. During the SPP, no such combination of tracers has been found.

- The benchmark reaction rate, which was used as a validation tool was limited to a single reaction, i.e. the oxidation of methane, due to its high importance in technical combustion applications. Further benchmarking should be performed using other, gaseous reactants. Special emphasis should be put on analyzing the influence of the Damköhler number on the model and the influence of the scalar dissipation rates on the reaction rate at higher Damköhler numbers.
- It should be tested whether the accuracy of the model could be further improved by implementing a full transport equation for both the scalar dissipation rates and the scalar cross dissipation rates.
- Further analysis of the influence on the sub-grid scalar dissipation rates and cross dissipation rates on the reaction rates is needed, especially at higher Reynolds numbers where the sub-grid scale models have more work to do.
- The influence of the mechanical-to-scalar time scale ratio needs to be assessed, since the spectra are not necessarily fully developed and a uniform value might not be appropriate.
- The population of the look up table should be optimized as well as its storage as currently only very simple algorithms are used.

Bibliography

[Bat59] G. K. Batchelor. Small-scale variation of convected quantities like temperature in turbulent fluid part 1. general discussion and the case of small conductivity. *Journal of Fluid Mechanics*, 5(01):113–133, 1959.

[Bat67] G. K. Batchelor. *An Introduction to Fluid Dynamics*. 1967.

[BGP04] M. Brandt, E. Gharaibah, and W. Polifke. Modellierung von Mischung und Reaktion in turbulenten Mehrphasenströmungen mittels Verteilungsfunktion. *Chemie Ingenieur Technik*, 76(01/Feb):46–51, 2004.

[BMPW10] Bockhorn, Mewes, Peukert, and Warnecke. *Micro and Macro Mixing*. 2010.

[Bot10] D. Bothe. Evaluating the quality of a mixture: Degree of homogeneity and scale of segregation. In Henning Bockhorn, Dieter Mewes, Wolfgang Peukert, and Hans-Joachim Warnecke, editors, *Micro and Macro Mixing – Analysis, Simulation and Numerical Calculation*, number ISBN 978-3-642-04548-6, pages 17–35. Springer Verlag, 2010.

[BP02] M. Brandt and W. Polifke. Tabulation of mean reaction rates from multivariate, correlated distributions with a monte carlo model. 9th Int. Conference on Numerical Combustion, page 2, Sorrento,Italy, 2002. SIAM.

[BPI+03] M. Brandt, W. Polifke, B. Ivancic, P. Flohr, and B. Paikert. Autoignition in a gas turbine burner at elevated temperature. Number 2003-GT-38224 in Proc. of ASME Turbo Expo 2003 Power for Land, Sea and Air, page 11, Atlanta, Georgia, USA, June 16-19 2003. ASME.

[Bra05] M. Brandt. *Beschreibung der Selbstzündung in turbulenter Strömung unter Einbeziehung ternärer Mischvorgänge*. PhD thesis, Technische Universität München, 2005.

[Cur63] R. L. Curl. Dispersed phase mixing: I. theory and effects in simple reactors. *AIChE Journal*, 9(2):175–181, 1963.

[CWP07] R. R. Cao, H. Wang, and S. B. Pope. The effect of mixing models in PDF calculations of piloted jet flames. Proceedings of the Combustion Institute, pages 1543–1550, 2007.

[DO74] C. Dopazo and E. E. Obrien. Approach to autoignition of a turbulent mixture. *Acta Astronautica*, 1(9-10):1239–1266, 1974.

[Dur07] L. Durand. *Development, implementation and validation of LES models for inhomogeneously premixed turbulent combustion*. PhD thesis, TU München, 2007.

[DVnF97] C. Dopazo, L. Valiño, and N. Fueyo. Statistical description of the turbulent mixing of scalar fields. *Int. J. Mod. Phys.*, B 11:2973, 1997.

[Eid85] Thomas M. Eidson. Numerical simulation of the turbulent Rayleigh-Benard problem using subgrid modelling. *Journal of Fluid Mechanics*, 158:245–268, 1985.

[EP88] V. Eswaran and S. B. Pope. Direct numerical simulations of the turbulent mixing of a passive scalar. *Physics of Fluids*, 31:506–520, 1988.

[FMP09] F. V. Fischer, B. Muralidharan, and W. Polifke. Simulation of ternary mixing in a co-annular jet in crossflow. *JSME Int. J., J. of Fluid Science and Technology*, 4(2):379–390, 2009.

[Fox03] Rodney O. Fox. *Computational Models for Turbulent Reacting Flows*. Cambridge, 2003.

[FP10] Frank Victor Fischer and Wolfgang Polifke. Formulation and validation of an LES model for ternary mixing and reaction based on joint presumed discrete distributions. In Henning Bockhorn, Dieter Mewes, Wolfgang Peukert, and Hans-Joachim Warnecke, editors, *Micro and Macro Mixing – Analysis, Simulation and Numerical Calculation*, number ISBN 978-3-642-04548-6, pages 185–204. Springer Verlag, 2010.

[Fri01] R. Friedrich. Strömungen verdünnter Gase. *TU München*, 2001.

[Fri02] R. Friedrich. Kompressible Strömungen mit Reibung und Wärmeleitung. *TU München*, 2002.

[Fri03] R. Friedrich. Grundlagen turbulenter Strömung und numerische Simulation. *TU München*, 2003.

[GB87] E. Gutheil and H. Bockhorn. The effect of multi-dimensional PDFs on the turbulent reaction rate in turbulent reactive flows at moderate Damköhler numbers. *PhysicoChemical Hydrodynamics*, 9(3/4):525–535, 1987.

[GM95] S. Ghosal and P. Moin. The basic equations of the large eddy simulation of turbulent flows in complex geometry. *Journal of Computational Physics*, 118:24–37, 1995.

[GO93] F. Gao and E. E. O'Brien. A large eddy simulation scheme for turbulent reacting flows. *Physics of Fluids A*, 5:1282, 1993.

[GPMC91] M. Germano, U. Piomelli, P. Moin, and W. H. Cabot. A dynamic subgrid-scale eddy viscosity model. *Physics of Fluids*, 3:1760–1765, July 1991.

[Gri77] U. Grigull. *Technische Thermodynamik*. De Gruyter, 1977.

[Gut91] E. Gutheil. Multivariate PDF closure applied to oxidation of CO in a turbulent flow. In A. L. Kuhl, J.-C. Leyer, A. A. Borisov, and W. A. Sirignano, editors, Dynamics of Deflagrations and Reactive Systems. *Progress in Astronautics and Aeronautics*, 1991.

[JDCB01] C. Jimenez, F. Ducros, B. Cuenot, and B. Bedat. Subgrid scale variance and dissipation of a scalar field in large eddy simulations. *Physics of Fluids*, 13:1748–1754, 2001.

[JJ79] W. Kollmann J. Janicka, W. Kolbe. Closure of the transport–equation for the probability denstiy function of turbulent scalar fields. *Journal of Non-Equilibrium Thermodynamics*, 4(1):47–66, 1979.

[Kim04] G. E. Kim. Large eddy simulation using unstructured meshes and dynamic subgrid-scale turbulence models. 34th AIAA Fluid dynamics conference and exhibit, pages 1–18, 2004.

[Kol41] A. Kolmogorov. The Local Structure of Turbulence in Incompressible Viscous Fluid for Very Large Reynolds' Numbers. *Akademiia Nauk SSSR Doklady*, 30:301–305, 1941.

[Kol62] A. Kolmogorov. A refinement of previous hypotheses concerning the local structure of turbulence in a viscous incompressible fluid at high Reynolds number. *Journal of Fluid Mechanics*, 13:82–85, 1962.

[Lea07] L. G. Leal. *Advanced transport phenomena: fluid mechanics and convective transport processes*. 2007.

[Leo74] A. Leonard. Energy cascade in large-eddy simulations of turbulent fluid flows. In *Turbulent diffusion in environmental pollution*, 1974.

[Lil92] D. K. Lilly. A proposed modification of the germano subgrid-scale closure method. *Physics of Fluids*, 4:633–635, 1992.

[Man04] M. Manhart. A zonal grid algorithm for DNS of turbulent boundary layers. *Computer and Fluids*, 33(3):435–461, 2004.

[Meu08] H. Meuer. The TOP500 Project: Looking Back over 15 Years of Supercomputing Experience. 2008.

[MJ04] D. W. Meyer and P. Jenny. Stochastic mixing model for pdf simulations of turbulent reacting flows. Tenth European Turbulence Conference, pages 681–684, 2004.

[MJ06] D. W. Meyer and P. Jenny. A mixing model for turbulent flows based on parameterized scalar profiles. *Physics of Fluids*, 18(3):035105, 2006.

[MTF01] M. Manhart, F. Tremblay, and R. Friedrich. MGLET: a parallel code for efficient DNS and LES of complex geometries. *Parallel Computational Fluid Dynamics 2001*, 2001.

[MV89] K. Mayberg and P. Vachenauer. *Höhere Mathematik 1*. 1989.

[Pet84] N. Peters. Laminar diffusion flamelet models in non-premixed turbulent combustion. *Progress in Energy and Combustion Science*, 10(3):319–339, 1984.

[Piq02] J. Piquet. La turbulence et sa modelisation. *Ecole Centrale de Nantes*, 2002.

[PM98] Ch. Pierce and P. Moin. A dynamic model for subgrid-scale variance and dissipation rate of a conserved scalar. *Physics of Fluids*, 10:3041–3044, 1998.

[Pop85] S. B. Pope. PDF methods for turbulent reactive flows. *Progress in Energy and Combustion Science*, 11:119–192, 1985.

[Pop91] S. B. Pope. Mapping closures for turbulent mixing and reaction. *Theoretical and Computational Fluid Dynamics*, 2:255–270, 1991. 10.1007/BF00271466.

[Pop94] S. B. Pope. Lagrangian PDF methods for turbulent flows. *Annual Review of Fluid Mechanics*, 26:23–63, 1994.

[Pop00] S. B. Pope. *Turbulent Flows*. Cambridge, 2000.

[PS00] H. Pitch and H. Steiner. Large-eddy simulation of a turbulent piloted methane/air diffusion flame (sandia flame d). *Physics of Fluids*, 12:2541–2554, 2000.

[PV05] T. Poinsot and D. Veynante. *Theoretical and Numerical Combustion*. Edwards, R. T. Incorporated, 2 edition, 2005.

[SM07] F. Schwertfirm and M. Manhart. DNS of passive scalar transport in turbulent channel flow at high Schmidt numbers. *International Journal of Heat and Fluid Flow*, 28:1204–1214, 2007.

[Sma63] J. S Smagorinsky. General circulation experiments with the primitive equations, part I: The basic experiment. *Monthly Weather Review*, 91:99–152, 1963.

[SP98] S. Subramaniam and S. B. Pope. A mixing model for turbulent reactive flows based on euclidean minimum spanning trees. *Combustion and Flame*, 115(4):487–514, 1998.

[Tay35] G. I. Taylor. Statstical theory of turbulence. Proceedings of the Royal Society, pages 421–464, 1935.

[TL87] H Tennekes and J. L. Lumley. *A First Course in Turbulence*. MIT Press, 1987.

[VD72] J. Villermaux and J. C. Devillon. Representation de la coalencence et de la redispersion des domaines de segregation dans un fluide par un modele dlinteraction phenomenologique. Second International Symposium on Chemical Reaction Engineering, pages 1–13, 1972.

[WW89] H. Werner and H. Wengle. Large-eddy simulation of turbulent flow over a square rib in a channel. In *7th Symposium on Turbulent Shear Flows, Volume 1*, volume 1 of *Thin Solid Films*, page 10, 1989.

[YH85] A. Yoshizawa and K Horiuti. A Statistically-Derived Subgrid-Scale Kinetic Energy Model for the Large-Eddy Simulation of Turbulent Flows. *J. Phys. Soc. Jpn.*, 54:2834–2839, 1985.

List of Figures

1.1 Schematic of the GT26 gas turbine, main flow is from right to left in this case 2
1.2 Schematic of a co-annular jet in cross flow. Main flow is from left to right. Left image displays the central jet, right image shows the annular jet 2
1.3 Work flow diagram of the basic idea in this thesis 5

2.1 Volume element of a fluid with the required physical quantities to describe the flow V: volume of the element S: surface of the element ρ: density e: internal energy w: heat production σ_i: shear stress p: pressure n_i: normal vector q_i: heat flux vector u_i: velocity vector g_i: volume force 12
2.2 Turbulent flow of exhaust and cooling gases during Space Shuttle mission STS-1 launch. Picture courtesy of NASA 21
2.3 The turbulent energy cascade 24

3.1 Initial distribution for the mixing model. Dashed line indicates the boundary of the physically accessible state-space: The sum of mixture fractions can never exceed unity 43
3.2 Distribution of mixing parameter for a single mixture fraction (left) and multiple mixture fractions (right). The area of both rectangles in the right case is identical. 47
3.3 Variance decay over mixing processes for the Modified Curl Model over a total of 400 mixing processes with 1600 particles. Both target variances are met after the same number of mixing events. The target variances for each mixing parameter is indicated by the horizontal line of the same color. 48
3.4 Example reaction rate of the first oxidization step of methane. Three streams are involved, one contains methane at 300K, the other two air at 600K and 1200K. 50

3.5 Distributions with different correlations taken from DNS. (a) Distribution with a low (absolute value) correlation, which is more circular in nature. (b) Distribution with a higher absolute value for the correlation, it is more elliptic. 50
3.6 Principle of covariance based mixing: As the blue particles are perpendicular to the reference slope (dashed line), they mix more rapidly as the brown particles, which are more in-line to the reference slope (mixing intensity indicated by arrow length) 52
3.7 Evolution of the covariance of a given distribution. The initial covariance is determined by the initial Dirac–Delta peaks, the targeted covariance is -0.2 53

5.1 DNS of a co-annular jet-in-crossflow, showing the mixture fractions for the two jets, main flow from left to right. (a) Mixture fraction of central jet. (b) Mixture fraction of annular jet. 70
5.2 DNS computation from MGLET, using 256x200x256 grid points,with one scalar shown on the left and the second scalar, corresponding to the annular jet, on the right. Main flow from left to right. 73
5.3 DNS of a jet-in-crossflow arrangement. Left is the two dimensional plot along the center of the channel, right is the one dimensional plot of the scalar along the line indicated on the left side. The out-of-bounds values can be seen clearly 73
5.4 Velocity profile in the inlet pipes of a co-annular jet-in-crossflow configuration, after half the length of the pipe 76
5.5 Sub-grid scale viscosity of an LES test run using a DNS grid to assess the resolution of the grid. The molecular viscosity of the computation is 3.55e-6. It can been seen that the contribution of the sub-grid scale model is between one and two orders of magnitude lower than the molecular viscosity, showing that the resolution of the DNS is sufficient 76
5.6 DNS post processing step to obtain *DNS distributions* 77
5.7 Scalar 1 (top) and Scalar 2 (bottom) of a DNS is co-annular jet-in-crossflow arrangement. 80
5.8 Stream wise slice of the co-annular jet-in-crossflow. (a) Scalar variance of mixture fraction 1. (b) Corresponding scalar dissipation rate 81

5.9 Stream wise slice of the co-annular jet-in-crossflow. (a) Scalar variance of mixture fraction 2. (b) Corresponding scalar dissipation rate 82
5.10 Stream wise slice of the co-annular jet-in-crossflow. (a) Covariance of the two mixture fractions. (b) Scalar cross dissipation rate 84
5.11 Mechanical-to-scalar time scale ratio of scalar 1 (top) and scalar 2 (bottom) 85
5.12 Side-by-side display of the mechanical-to-scalar time scale ratio and the mean of the same scalar. (a) Mechanical to scalar time scale ratio. (b) mean value of the mixture fraction. 86
5.13 Comparison of the sub-grid scalar dissipation rate of scalar 1. Left reference data obtained by filtering DNS, right the LES model . . 87
5.14 Comparison of the sub-grid scalar dissipation rate of scalar 2. Left reference data obtained by filtering DNS, right the LES model . . 87
5.15 Comparison between distributions. Distributions generated by mixing models are displayed in the left column, those taken from the DNS data are shown in the right column. The distributions in one row have the same statistical moments. One scalar fraction depicted on the the X–axis, the other on the Y–axis. Red lines indicate the boundary of the physical space, so that the sum of scalar fractions does not exceed unity. In each case, the resulting reaction rate differs by less than 5%. 89
5.16 Example reaction rate over the number of mixing processes. Means are conserved, Variances decay from left to right. Large differences can be seen between distributions of different correlations. Blue line: negative correlation of -0.4; Green line: positive correlation of +0.4 90
5.17 Reaction rate dependency for a given distribution. 92

Appendix A

Derivation of the Covariance

$$\iint \left[\Gamma_1 - \overline{\phi}_1\right] \left[\Gamma_2 - \overline{\phi}_2\right] d\Gamma_1 d\Gamma_2 = \tag{A.1}$$

$$= \iiint \left[\Gamma_1 - \overline{\phi}_1(x)\right] \left[\Gamma_2 - \overline{\phi}_2(x)\right] G\left(x,x'\right) \delta\left(\Gamma_1 - \phi_1(x')\right) \delta\left(\Gamma_2 - \phi_2(x')\right) \tag{A.2}$$

$$d\Gamma_1 d\Gamma_2 dx' =$$

$$= \int \left[\phi_1(x')\phi_2(x') - \overline{\phi}_1(x)\phi_2(x') - \phi_1(x')\overline{\phi}_2(x) + \overline{\phi}_1(x)\overline{\phi}_2(x)\right] G\left(x,x'\right) dx' = \tag{A.3}$$

$$= \overline{\phi}_1(x)\overline{\phi}_2(x) + \overline{\phi_1(x)\phi_2(x)} - \overline{\overline{\phi}_1(x)\phi_2(x)} - \overline{\phi_1(x)\overline{\phi}_2(x)} = \tag{A.4}$$

$$= \overline{\phi_1(x)\phi_2(x)} - \overline{\phi}_1(x)\,\overline{\phi}_2(x). \tag{A.5}$$

Appendix B

Quality of Mixing

In the SPP1141, within which this thesis was written, it became quickly apparent that no generally accepted definition of the quality of a mixture exists. This was especially true in an environment where a large number of different reactors with a considerable difference in physical size, throughput and Reynolds numbers were examined. The final publication of the SPP1141 [BMPW10] dedicates a separate section to exactly this problem. A brief overview of these findings will be shown here.

Bothe [Bot10] displays that the *variance* of a mixture fraction or concentration proves to be a good measure for the quality of the mixing process especially for reacting mixtures. However, he also explains that the variance is completely independent from the *scale of segregation* of the mixture. To adequately describe a mixture, the analysis of both these parameters appears to be required.

For the homogeneity of a mixture, it is shown that

$$\frac{\text{rate of reaction at given conditions}}{\text{rate of reaction for homogeneous mixture}} = 1 + \frac{Cov(c_A, c_B)}{\langle c_a \rangle \langle c_B \rangle}, \tag{B.1}$$

which contains the covariance *Cov* of the concentrations.

It is also shown that for the given configuration, which is a T-shaped mixer, the integral length scale of the scale of segregation depends on the Schmidt number, while the smallest length scales depend on the Batchelor length scale. The scale of segregation itself represents the total surface area as in

$$|\Gamma| = \int_V ||\frac{\partial f}{\partial x_i}|| dV, \tag{B.2}$$

with Γ as the surface area and the term $||\frac{\partial f}{\partial x_i}||$ as the Euclidean length of the gradient of f. In summary, Bothe suggests to put more emphasis on integral measures of the scaled which have been produced by the mixing process.

Appendix C

Implementation of the Transport Equations in OpenFOAM

The following is the implementation of the second order moments transport equations in OpenFOAM including the model for the dissipation rates.

```
dub = 2 * (sgsModel->nu() + sgsModel->nuSgs()) /
    (0.7 * 0.06 * sqr(sgsModel->delta()));
chi1 = tTurb * f1var;

fvScalarMatrix f1varEqn (
  fvm::ddt(f1var)
 + fvm::div(phi, f1var, "div(phi,fvar)")
 - fvm::laplacian( (D + sgsModel->nuSgs()),
       f1var, "laplacian(D,f)")
 -  2 * (D + sgsModel->nuSgs()) *
       (fvc::grad(f1) & fvc::grad(f1))
 +  chi1
);
f1varEqn.relax();
f1varEqn.solve();

chi2 = tTurb * f2var;

fvScalarMatrix f2varEqn (
  fvm::ddt(f2var)
 + fvm::div(phi, f2var, "div(phi,fvar)")
 - fvm::laplacian( (D + sgsModel->nuSgs()),
        f2var, "laplacian(D,f)")
 - 2 * (D + sgsModel->nuSgs()) *
      (fvc::grad(f2) & fvc::grad(f2))
 +  chi2
);
```

```
f2varEqn.relax();
f2varEqn.solve();

cross_chi12 = tTurb * f1f2cov;

fvScalarMatrix f1f2covEqn (
  fvm::ddt(f1f2cov)
 + fvm::div(phi, f1f2cov, "div(phi,fvar)")
 - fvm::laplacian( (D + sgsModel->nuSgs()),
       f1f2cov, "laplacian(D,f)")
 - 2 * (D + sgsModel->nuSgs()) *
      (fvc::grad(f1) & fvc::grad(f2))
 + cross_chi12
);
f1f2covEqn.relax();
f1f2covEqn.solve();
```